383

Assimilation and Modelling of the Hydrological Cycle: ECMWF's Status and Plans

E. Hólm, E. Andersson,
A. Beljaars, P. Lopez, J-F. Mahfouf,
A. Simmons and J-N. Thépaut

Research Department

ECMWF

September 2002

Abstract

Several new types of satellite instrument will provide a rich source of additional humidity information in the next few years. The assimilation of cloud and rain observations from existing types of instruments will also provide important new humidity information. In an effort to make the best possible use of these data a re-formulation of the 4D-Var humidity analysis has been developed. The new formulation will better account for the wide variations in humidity in the vertical and at small scales in the horizontal, thus improving the interpretation and the spatial interpolation of humidity information from space and ground based observing systems. The theoretical basis for the new formulation, its practical implementation within the ECMWF assimilation system, and several illustrations of its performance, are presented. The status of the preparations for cloud and rain assimilation is given, including the development of linearized moist physics, the development of fast radiative transfer codes and the recent experimental results using rainfall rates from space borne microwave radiometers.

Results of model validations (against *in-situ* data) of boundary-layer moisture are presented, indicating generally good agreement — often to within the absolute calibration accuracy of the measurements. We also present evidence of shortcomings in ECMWF's current humidity analysis, from the operational data assimilation and forecasting system, and from the 40-year reanalysis project (ERA-40). Examples are shown of biases in the data and in the model that lead to biased humidity analyses. Although these biases are relatively small, they contribute to an over-prediction of precipitation in short-range forecasts and a marked spin-down in tropical rainfall.

1 Introduction

The main space agencies (ESA, NASA, NASDA) have a number of Earth observation missions with the objective of providing improved measurements of the global hydrological cycle: clouds (CloudSat, CALIPSO, EarthCARE), precipitation (TRMM, GPM) and soil moisture (SMOS). Significant development of the 4D-Var system will be necessary for optimal use of both the existing and these new types of observations of the water cycle. The notable small-scale variability in atmospheric humidity and its strong interactions with physics and dynamics need to be represented accurately in the assimilation system. In this paper we report on the progress with cloud and rain assimilation, using data from TRMM and SSMI, and on the formulation of a new humidity analysis. We also illustrate some shortcomings of the current humidity analysis, in its operational configuration and in the context of ECMWF's 40-year reanalysis (ERA-40).

The 4D-Var humidity analysis is structurally fully integrated with the analysis of the dynamic variables (temperature, surface pressure, vorticity and divergence (Courtier *et al.* (1994), Courtier *et al.* (1998)) thereby providing scope for realistic interactions. Interaction takes place at 4D-Var inner-loop level through advection, and through the processes parameterized in the linearized physics (Janisková *et al.* (2000), Janisková (2001)). At 4D-Var outer-loop level further interaction between temperature, wind and humidity takes place as the full high-resolution non-linear model is used to propagate the analysis increments over the 12-hour assimilation time window (Bouttier (2001)). There is also an important interaction introduced through the observation operators (at inner and outer loop) for those observations that involve both humidity and temperature, e.g. humidity-sensitive infra-red and microwave radiances, cloud and precipitation data.

Within the 4D-Var background term, on the other hand, the current humidity analysis lacks direct coupling between specific humidity and the dynamic variables. Such coupling can be introduced either through a careful choice of humidity control variable (other than specific humidity), or through the application of analytical or statistical correlations (Derber and Bouttier (1999)). The choice of control variable is central to the humidity analysis (Dee and Da Silva (2002)) as it can influence also the conditioning of the analysis problem, and improve its behaviour near the physical bounds for humidity: zero and saturation.

From experience with the operational system at ECMWF, several important shortcomings of the current humidity analysis have been identified. Some are due to small but significant biases between the forecast model and the observational data (Section 2). These biases likely contribute to the now well-known spin-down of precipitation in the short-range forecasts and in the ERA-40 reanalyses (Section 3).

The availability of humidity observational information for the purpose of global NWP and climate simulations is very incomplete. Existing satellite systems (HIRS, METEOSAT and SSMI) provide valuable information (Section 4), but this information is limited by its poor vertical resolution. Many data types, including the conventional data from radiosondes and SYNOP stations, are affected by significant random errors and biases. We should not forget, however, that the situation has improved very substantially compared to the late 1980s (Illari (1989)) when satellite humidity information (in the form of statistical retrievals of integrated water content in three layers) was first used in ECMWF's then operational OI (Optimal Interpolation) data assimilation system.

For the immediate future, it is expected that the AIRS instrument on NOAA's AQUA satellite (launched in June 2002) will provide a very substantial increase in available humidity information, with a nominal accuracy of 20% in 1 *km* thick layers and twice daily global coverage, to be followed a few years later by IASI on METOP. The preparation for the use of AIRS and IASI data in NWP is well advanced, e.g. through the work co-ordinated by EUMETSAT within the NWP-SAF (Satellite Application Facility for Numerical Weather Prediction). A fast radiative transfer model for AIRS is already available in the current version of RTTOV-7 (Saunders *et al.* (1999)). For IASI, there is RTIASI developed by Matricardi and Saunders (2001).

A fast microwave radiative transfer model for clouds and precipitation (including scattering effects) has been developed (Bauer (2002)) and evaluated (Moreau *et al.* (2002)). With the availability of these tools and with additional upgrades of the 4D-Var solution algorithm itself, direct radiance assimilation of cloud and rain affected radiances will be possible (Section 5). The alternative approach to assimilate in 4D-Var total-column water-vapour, obtained through a 1D-Var algorithm using satellite measurements of rainfall rate from SSMI and TRMM, has been studied by Marécal *et al.* (2002a), Marécal *et al.* (2002b), Marécal and Mahfouf (2002a) and Marécal and Mahfouf (2002b).

An issue specific to humidity is the large variability of the background-error variances on small spatial scales, making the interpolation of humidity information a delicate problem. The development of the humidity analysis has in several respects lagged behind that of the mass and wind analysis: The current background constraint is uni-variate in specific humidity. The background-error variances are not cycled but are, in contrast to the other variables, given through an empirical relationship with T and q of the background state (Rabier *et al.* (1998)). The revised humidity analysis presented in Section 6 addresses some of these issues. The section is devoted to the new formulation of the humidity analysis, providing a description and a collection of early results. Some single-observation tests and tests with real METEOSAT and SSMI radiances data show promising results. Work with AIRS and SSMI/S will commence as soon as data become available. The assimilation of AMSU-B data will also be investigated.

The plan of the paper is as follows: In Section 2 we present examples of model verification to give some insight into the realism and quality of the humidity fields provided by the ECMWF model. In Section 3 we investigate possible causes for the excessive tropical rainfall rates seen in the short-range ERA-40 and operational forecasts. Results show that the hydrological cycle in the tropics is strongly influenced by the assimilation of SSMI total-column water-vapour data, and HIRS radiances. We report on the progress with the assimilation of new and planned satellite humidity data in Section 4, and on the progress with the assimilation of cloud and precipitation data in Section 5. The work on the re-formulation of the humidity analysis, and the possibilities for further improved background-error modelling, is described in Section 6. Results from tests with global sets of METEOSAT and SSMI radiance data, using the re-formulated humidity analysis are also presented. Conclusions are drawn in Section 7.

2 Modelling aspects and validation against in-situ data

Moist processes are important for the modelling of clouds, precipitation, radiation and latent heat release. Furthermore, data assimilation relies heavily on the moisture field, not only as a background field for the moisture analysis but also in the retrieval of temperature information from satellite channels that are affected by moisture.

So how good are the moisture fields in the ECMWF model? The moisture field depends on physical parametrizations which can have substantial uncertainties, but it also depends on the large-scale motion, particularly the vertical motion. Strong sensitivity of atmospheric moisture to parametrization has been demonstrated in earlier work with the ECMWF model by e.g. Tiedtke *et al.* (1988) and Gregory (1996) for sensitivity to shallow convection, Tiedtke (1993) for sensitivity to cloud parametrization, Jakob and Klein (1999) for sensitivity to microphysics, and by Beljaars and Viterbo (1998) for the impact of boundary layer top entrainment and air-sea transfer.

This section does not provide a full review on all modelling aspects that affect moisture. Instead a few examples of verification will be presented to give some insight on the realism and quality of the ECMWF model.

2.1 Comparison to analysis, and evidence of spin-down in tropical precipitation

An obvious way of assessing the model is by looking at systematic errors as differences between forecasts and analyses. The monthly averaged difference for the month of April 2002 is shown in Fig.1 for day 1, day 2 and day 5 forecasts. The main difference is in the tropics where the model is drier than analysed. This is associated with a spin-down of precipitation in the tropics (Fig. 2) and a spin-down of the Hadley circulation as can bee seen from the systematic difference in vertical velocity (ω) between forecasts and analysis (Fig.3). Because of the additional latent heat release in the tropics during the first 12 hours of the forecasts, the Hadley circulation is stronger in the analysis than in the forecasts. It is important to note that the differences in relative humidity (Fig 1) between forecasts and analysis are up to about 5%, which is fairly small. At this stage it is difficult to say whether the model or the analysis is biased, because most current observing systems do not have an absolute calibration within 5%. In spite of the small imbalance in moisture between model and forecasts, the spin-down is damaging to the analysis as it maintains a too active hydrological cycle during the data assimilation.

2.2 Boundary-layer moisture over the oceans

Boundary-layer moisture is an important aspect of the model for two reasons: Firstly, together with surface wind speed it controls the surface evaporation, secondly, boundary-layer moisture is the dominant contribution to vertically integrated (total-column) water vapour (TCWV). The latter aspect is important in the context of microwave satellite observations, which provide good estimates of TCWV. An example is given in Fig.4 where the model first guess (top) is compared to 1D-Var retrievals (Phallipou (1996)) and to a model-independent retrieval using the algorithm of Alishouse *et al.* (1990). The patterns in the three panels are remarkably similar suggesting that the observations have a high degree of realism and that the physics and the dynamics of the model do a reasonable job. However, there is again a small systematic difference between the observations and the model. The difference is about $0.5\,kg/m^2$ in the global average, corresponding to about 2% of the global mean of $27\,kg/m^2$. Such a mismatch is small and may be due to a model bias or due to a bias in the observing and retrieval systems.

Boundary-layer moisture is an indirect indicator for the activity of processes at the top of the boundary layer. If we think of the marine boundary layer as a reasonably well-mixed reservoir with fluxes from the surface and
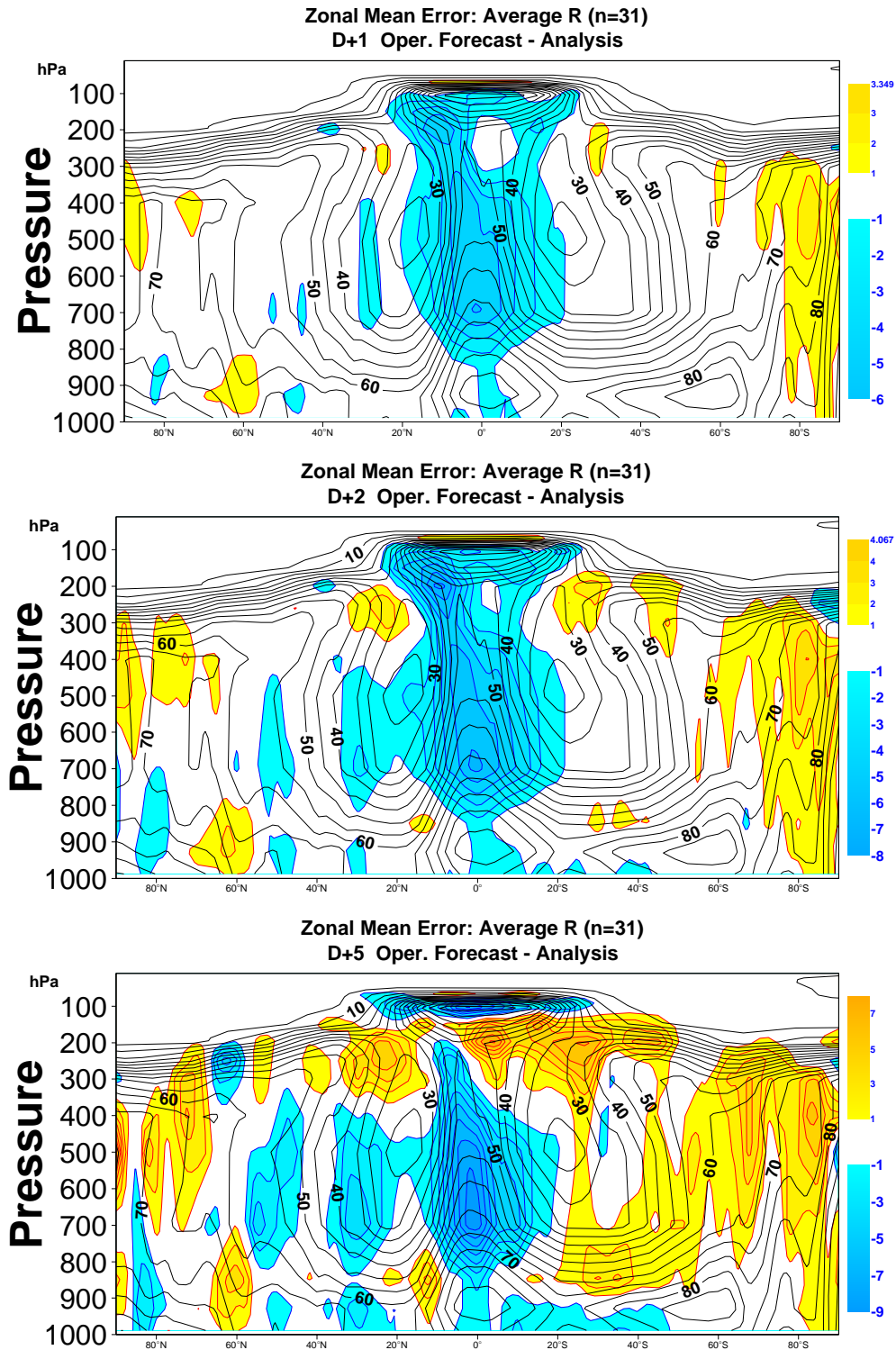
Zonal Mean Error: Average R (n=31)
D+1 Oper. Forecast - Analysis

Zonal Mean Error: Average R (n=31)
D+2 Oper. Forecast - Analysis

Zonal Mean Error: Average R (n=31)
D+5 Oper. Forecast - Analysis

Figure 1: Colour coded differences in relative humidity (%) between day 1 (top), day 2 (middle) and day 5 (bottom) forecasts and verifying analyses averaged over the month of April 2002 from the operational system. The averaged relative humidity (%) from the analysis is represented as a background field in black contours (contour interval 5%).
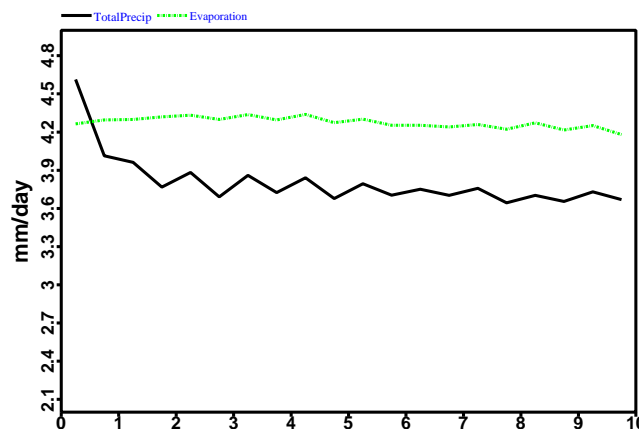
Figure 2: Evolution of precipitation (black line) and evaPoration (green) in the tropical band between 30 ^{o}N and 30°S during the 10-day forecasts from the operational system, averaged over the month of April 2002, in mm/day.

fluxes at the top, then the mixed-layer equilibrium value of specific humidity is determined by both processes. Since air-sea transfer is fairly well known, errors in boundary-layer specific humidity are most likely associated with errors in inversion interaction (e.g. through shallow convection). Field campaigns provide a valuable source of data to verify boundary-layer moisture. Often these observations are not used in the data assimilation, so they are particularly valuable for model validation. An example is the IMET ocean buoy system operated by the Woods Hole Oceanographic Institute (Weller and Anderson (1996)). In Figs. 5 and 6, the saturation specific humidity at the sea surface minus the observed specific humidity at 3.2 m height is compared with short-range forecasts of the ECMWF model. One of the so-called PACS buoys is located in the Pacific at 3°S 125°W; the IMET-Stratus buoy is located in a nearly permanent stratocumulus area at 20°S 85°W. Fig. 5 displays a time series over 17 months with 6-hour intervals. In general the correspondence is quite good, with the model being slightly too dry (i.e. the difference with the ocean surface being too large). This is more pronounced during the last five months when the sea-surface temperature drops gradually and the humidity difference with the ocean drops because warm moist air is advected over the relatively narrow cold tongue in sea-surface temperature that develops near the PACS buoy. The reason for these larger discrepancies in stably stratified situations over the ocean are not known. Comparison of the wind speed and surface fluxes (not shown) indicates very good agreement. This suggests that convection parametrization provides a realistic level of boundary-layer ventilation — otherwise bigger errors would be seen in near-surface moisture.

Also the time series (Fig. 6) for 17 days of hourly data from the IMET-Stratus location shows very good agreement between model and observations. It can again be concluded that the entrainment at the top of the cloudy boundary layer must be reasonable — otherwise near-surface moisture would be more biased.

The boundary-layer specific humidity is of course only one aspect of TCWV. The second major factor controlling TCWV is the boundary-layer depth. During the EPIC experiment, radiosondes were launched from a ship near the IMET-Stratus buoy. A comparison of averaged sondes and model profiles is shown in Fig.7. The most noticeable characteristic of these profiles is the sharp inversion which is the result of a subtle balance between large-scale subsiding motion and turbulent entrainment at the top of the cloud layer in the inversion. The model inversion is less sharp than the observed one and the model boundary-layer is lower than observed. This has consequences for TCWV because in this situation, TCWV is to a good approximation equal to the boundary-layer depth multiplied by the boundary-layer specific humidity. So relative errors in both parameters cause the same relative error in TCWV. Still the inversion structure is remarkably well captured, which implies that the model manages to maintain a reasonable balance between vertical advection and entrainment processes despite the limited vertical resolution, the long integration time steps and shortcomings of the parametrization.
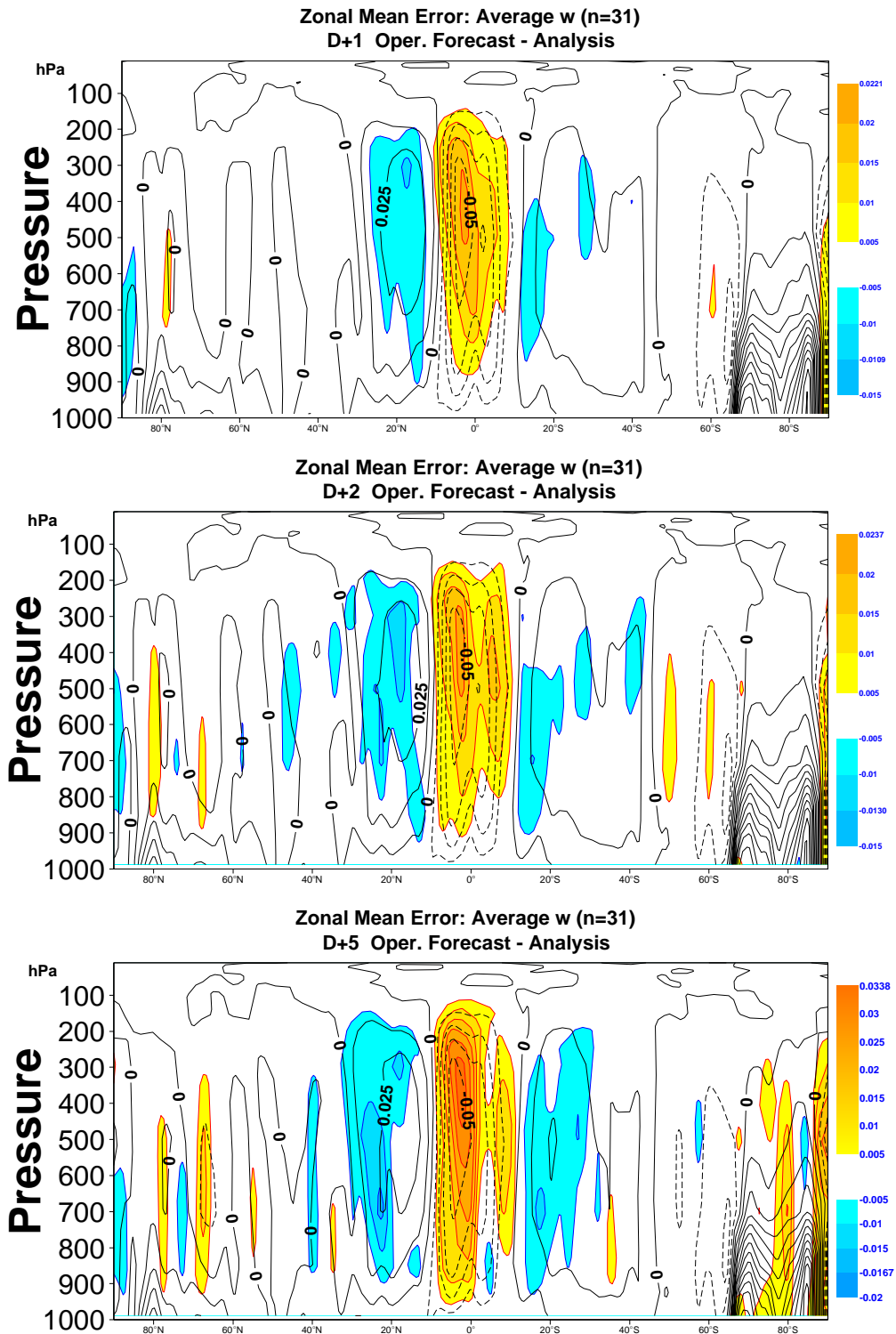
Zonal Mean Error: Average w (n=31)
D+1 Oper. Forecast - Analysis

Zonal Mean Error: Average w (n=31)
D+2 Oper. Forecast - Analysis

Zonal Mean Error: Average w (n=31)
D+5 Oper. Forecast - Analysis

Figure 3: Colour coded differences in vertical velocity (Pa/s) between day 1 (top), day 2 (middle) and day 5 (bottom) forecasts and the verifying analyses averaged over the month of April 2002 from the operational system. The averaged analysis is plotted as a background field (contour interval 0.025 Pa/s). The shading of the difference starts at $\pm 0.005\,Pa/s$ with a contour interval of 0.005 Pa/s.

2.3 Boundary-layer moisture over land, and the influence of the land surface

Boundary-layer moisture over land is very much affected by land surface processes through evaporation from the surface. This sensitivity has frequently been evident during work on the land surface scheme see e.g. Viterbo and Beljaars (1995) and Van den Hurk *et al.* (2000)). Summer precipitation over land is strongly influenced by land evaporation, which involves a positive feedback: high precipitation leads to more soil moisture, which enhances evaporation feeding back into high precipitation (Beljaars *et al.* (1996)). To control this positive feedback it is necessary to have a good soil moisture data assimilation scheme. Significant work has been done in the past (Viterbo and Courtier (1995) and Douville *et al.* (2000)) to optimize the use of SYNOP observations. Currently the EU-funded ELDAS project is underway to improve further the use of SYNOP data and to accommodate other data sources: radiation, precipitation, surface skin temperatures from satellites and future microwave data.

An area where the contrast between dry and moist is probably more pronounced than anywhere else is at the edge of the ITCZ over Africa. Over a distance of a few hundred kilometres boundary-layer moisture varies dramatically due to changing soil moisture conditions. From operational verification it is known that the ECMWF model has the northern edge of the ITCZ over West Africa displaced slightly too far south. Also the cirrus outflow tends to be underestimated. To illustrate the sharp gradient in boundary-layer moisture a time series of 2m specific humidity is shown for 4 latitude bands over Ghana (Fig. 8). The choice of time and place is inspired by the availability of heat flux observations near Tamale (Ghana) during December 2001. Figure 9 shows a comparison of observed heat fluxes with 12-36 hour forecasts in 3-hourly intervals. The good correspondance suggests that the partitioning of sensible and latent heat fluxes is reasonable, which implies that soil moisture also must be realistic. The north-south gradient in specific humidity is remarkable, both in model and observations. At the most southern band, the model is too dry, which is consistent with a slightly too southerly positioning of the rain in the model. In the middle two bands (at the transition from dry to wet), the station to station variability is very large. However, it was found that the gridpoint to gridpoint variability in the model is not significantly higher there than it is in the most northerly or most southerly area. The reason for the variability in the observations is most likely the patchiness of the rain, which is not faithfully reproduced by the model. This illustrates some of the difficulties and challenges posed by modelling and assimilation of atmospheric moisture and soil moisture. Globally uniform structure functions will certainly not apply in areas with such strong gradients in mean and variability.

2.4 Comparison to radiosondes over the western Pacific

The ARM programme maintains a few locations with very advanced high-quality observations. ECMWF collaboration with the ARM programme has already given interesting results. Christian Jakob (ARM fellow at BMRC, Australia), has compared output of the ECMWF model column for Manus ($147.4^o E \, 2.1^o S$), and Nauru ($166.9^o E \, 0.5^o S$) in the Western Pacific with radiosonde observations. The profiles are averaged according to precipitation classes as seen in the model during the one-hour period before the observation. The four panels in Fig. 10 show observed moisture profiles, modelled moisture profiles, and their differences all stratified according to precipitation rate. The 4th panel shows the precipitation frequencies in the different classes. A few conclusions can be drawn:

- The model rains too frequently. Although one has to be careful comparing a grid-average to a single point (as is well known from precipitation verification studies, Cherubini *et al.* (2001)), the difference is
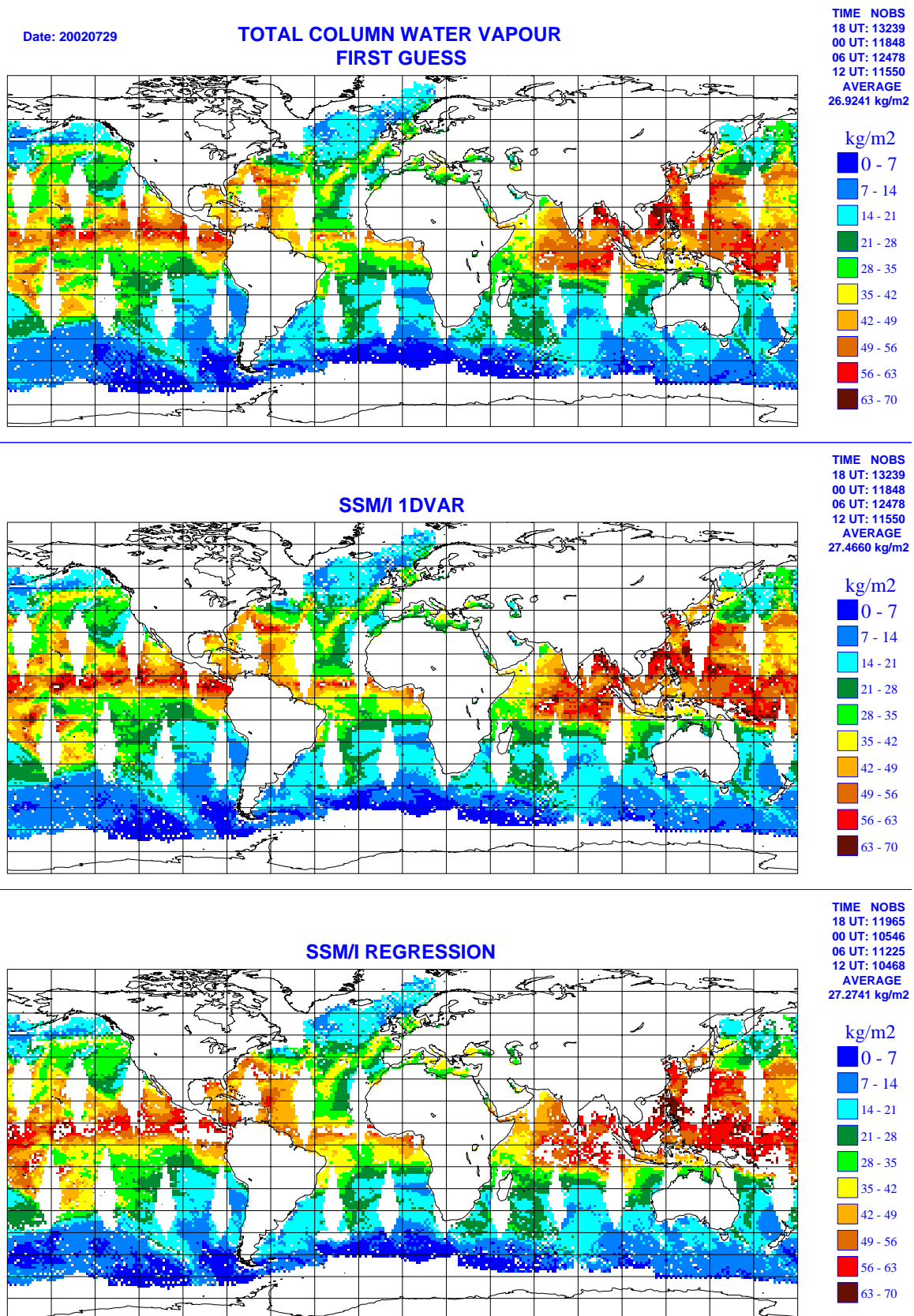
Figure 4: Total-column water-vapour (kg/m^2, see legend) from the model first guess (top), the 1D-Var retrieval (Phallipou (1996), middle), and a model-independent retrieval algorithm (Alishouse *et al.* (1990), bottom) for 29 July 2002.
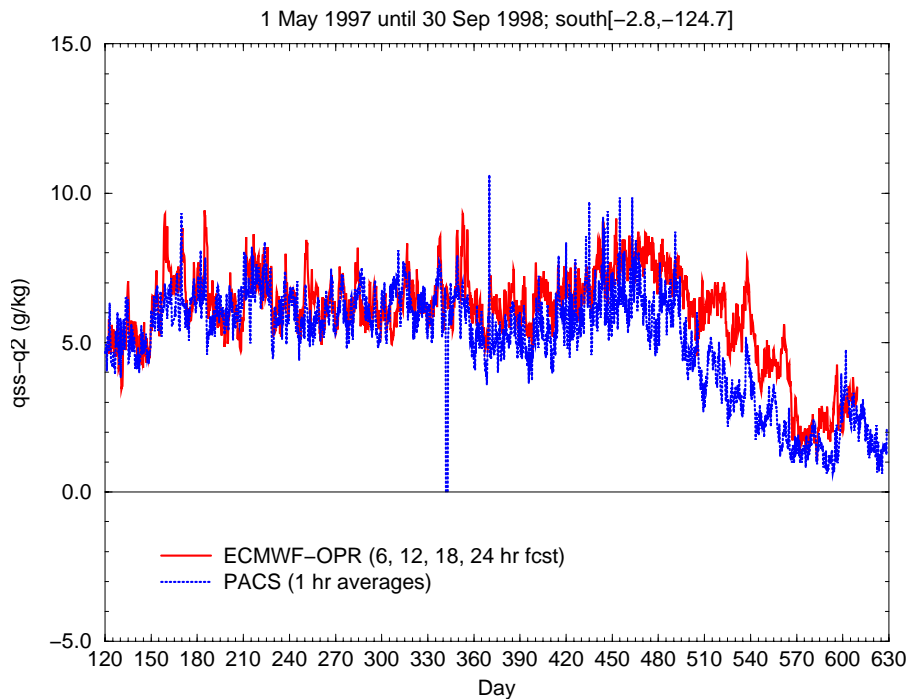
Figure 5: Time series over 18 months with 6-hour intervals of specific-humidity difference between the ocean surface and the 3.2 m level for the PACS buoy location $3^oS\,125^oW$. The model curve (red) is from daily forecast steps 6, 12, 18 and 24 hours. The buoy data (shown in blue) was kindly provided by the Woods Hole Oceanographic Institute.
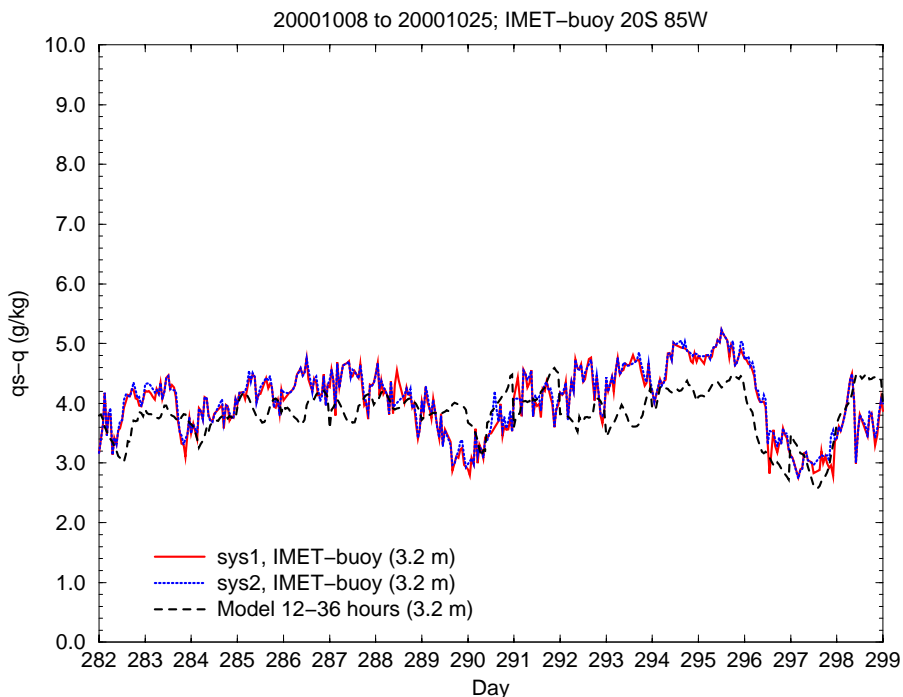

Figure 6: Time series over 17 days with one-hour intervals of specific humidity difference between the ocean surface and the 3.2 m level for the Stratus location $20^oS\,85^oW$. Two observing systems are shown (blue and red lines), giving virtually identical results. The model curve (black dashed line) is from daily forecast steps 12 to 36 hours. The buoy data was kindly provided by the Woods Hole Oceanographic Institute.
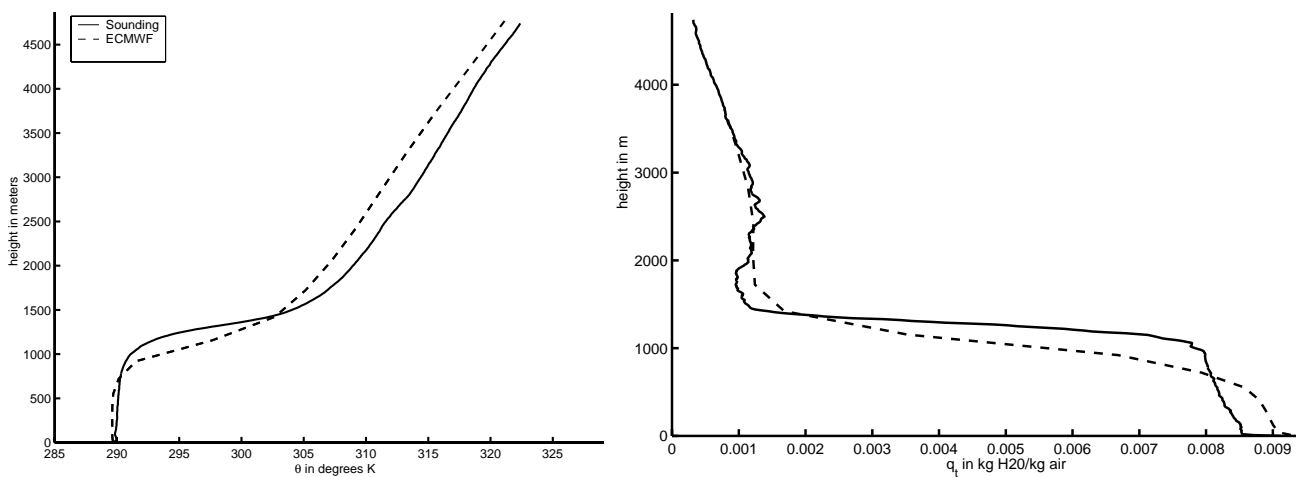
Figure 7: Average of radiosonde observations (full lines) during 6 days of potential temperature and specific humidity at the Stratus location $20^oS\,85^oW$. The corresponding averages of short-range forecasts (dashed) are also shown. The figure was kindly provided by Chris Bretherton, University of Washington.
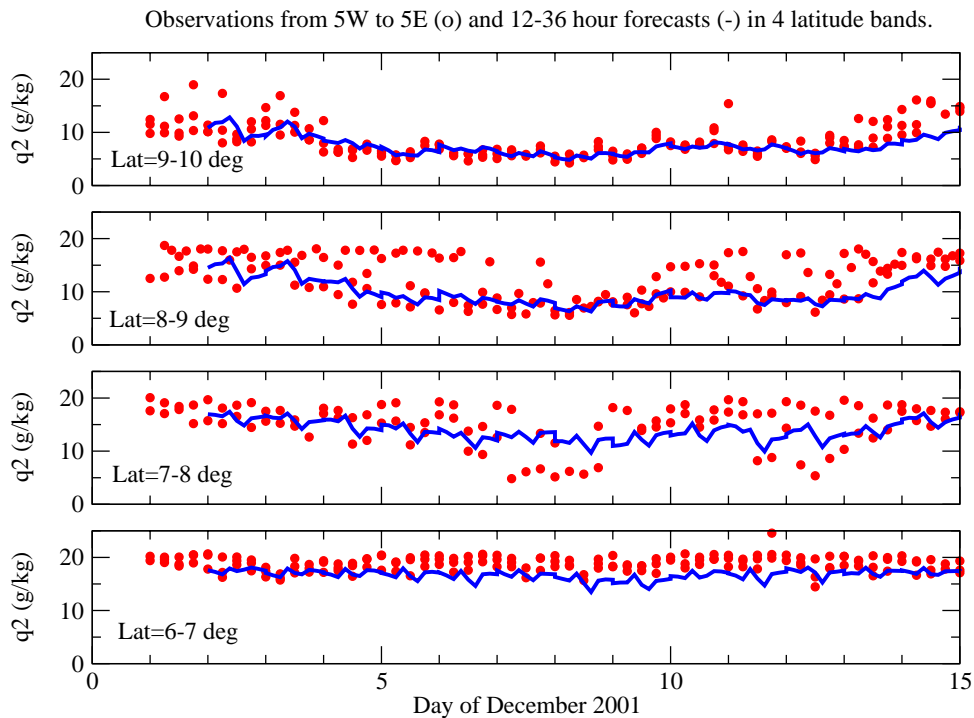

Figure 8: Time series for 2 weeks in December 2001 of 2m specific humidity in 4 latitude bands of 1° averaged from 5^oW to 5^oE. All the SYNOP stations in these bands are represented by the individual dots. The solid line represents the model averaged over the appropriate latitude band (12 – 36 hour daily forecast have been used with 3 hour intervals).

so large that the signal might be real - especially as the model is overestimating even the frequency of the larger precipitation amounts. The problem is larger at Nauru (the drier site in reality) than at Manus.

- The model shows a much smoother transition in RH from not rainy to rainy cases than the data. This is less obvious at Nauru, but here the sample size in the observations (see blue bars) for rain events is very small. At Manus, where the sample is bigger, there only seems to be a difference between rain and no-rain cases in the data. The model, however, shows substantial variation in humidity dependent on the
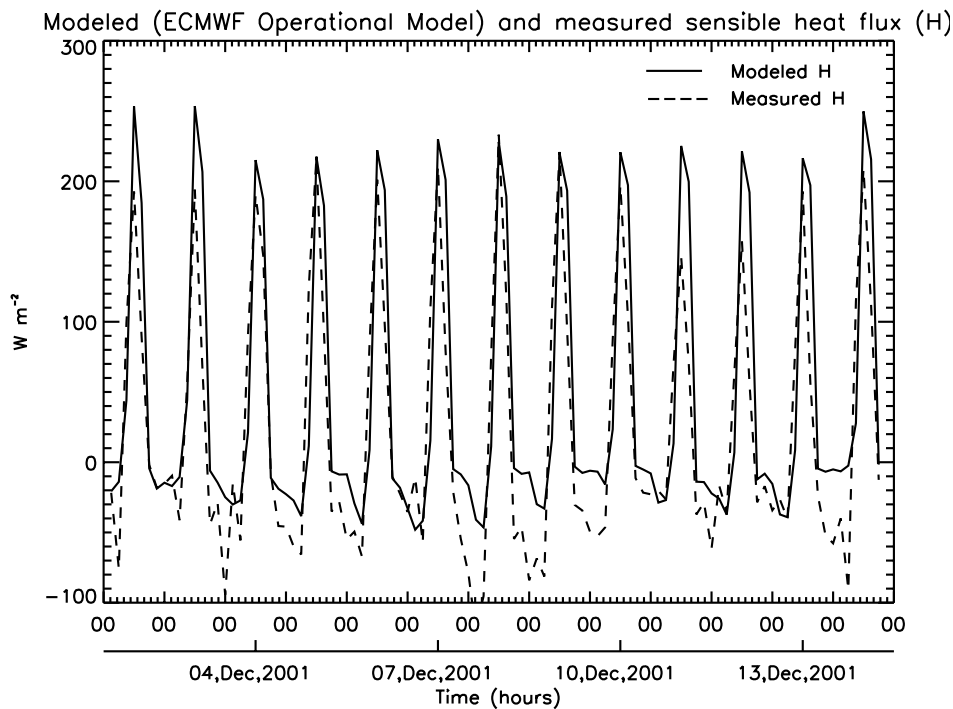
Figure 9: Time series for 2 weeks in December 2001 of observed surface heat flux (dashed) and modelled flux (solid) at Tamale (Ghana, $0.7^oW\,9.4^oN$). The model data is from 12 – 36 hour forecasts of the operational ECMWF model. This figure was kindly provided by Dirk Burose, University of Wageningen.

amount of rain.

- Boundary-layer moisture in the model seems to respond too much to rain. This may be related to the convection parametrization, but also to the efficiency of evaporation. Experience with the parametrization of precipitation fraction (Jakob and Klein (1999)) shows that boundary-layer moisture is sensitive to the evaporation of precipitation and to the fractional area over which this process occurs.

- Overall the model seems to be too dry (except in the boundary layer), which might be consistent with too much rain. In the classic Kuo convection scheme, the key parameter was how much of the moisture convergence would go into rain and how much into moistening the atmosphere. The more advanced mass flux parametrizations provide this implicitly through microphysics and the detrainment terms.

2.5   Concluding remarks about model and observation uncertainties

In this section a few examples have been shown of the capability of the ECMWF model to represent atmospheric moisture. Operational analyses and different observing systems have been used as reference. The general feeling is that the model uncertainty in moisture is of the same order as the uncertainty in the observations. The tropical spin-down during the first 12 hours of the forecasts represents a mismatch between analysis of moisture and the model climate, but the imbalance is within the absolute calibration accuracy of current moisture observing systems. Therefore, the spin-down can presently be reduced only by 'empirical bias correction'. Research quality data from field campaigns has already demonstrated its value for model improvement, and will become increasingly important in optimizing models and analysis systems.
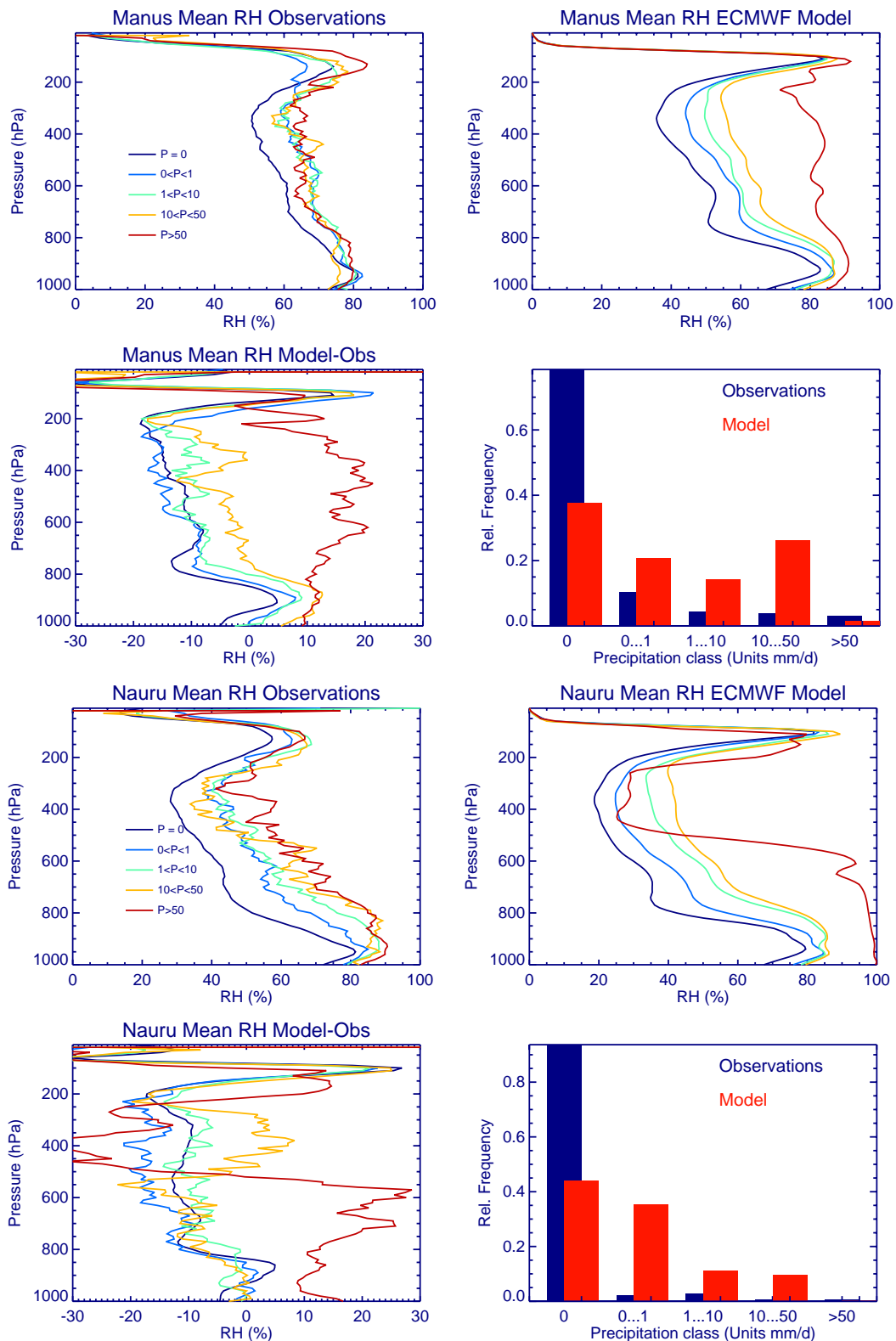
Figure 10: Radiosonde versus model comparison covering two years with averaging according to precipitation rate classes from the model during 1 hour before the observation. The top 4 panels are for Manus (147.4 ^oE 2.1^oS), the bottom panels for Nauru (166.9^oE 0.5^oS). The 4 panels show observed relative humidity, modeled relative humidity, difference in relative humidity between model and observation and precipitation frequency. The precipitation classes are: 0, 0-1, 1-10, 10-50 and > 50 mm/day. This figure was kindly provided by Christian Jakob, BMRC, Melbourne.

3   The tropical humidity analysis in ERA-40

The ERA-40 analyses are being produced in three streams that can be characterized in terms of the observations that influence the humidity analysis. In Stream-1, from 1987 onwards, *in-situ* surface (SYNOP) and radiosonde measurements, humidity-sensitive HIRS infra-red radiances and 1D-Var retrievals of total-column water-vapour from SSMI radiances are all assimilated. Stream-2 starts in 1957, and has only the conventional *in-situ* measurements available. Stream-3 uses the *in-situ* measurements and infra-red radiances, but not SSMI data. The infra-red data are from VTPR instruments from 1973 to 1978 and from HIRS instruments beyond 1978.

Diagnosis of hydrological aspects of the ERA-40 products has been carried out primarily by Stefan Hagemann and Klaus Arpe of the Max Planck Institut für Meteorologie (MPI), Hamburg, and by the ECMWF project team. These studies have shown some pronounced differences in the behaviour of the three streams that are almost certainly related mainly to the changes in data used rather than to natural earth-system changes.

3.1   The hydrological budget

Components of the global hydrological budget for each of the three streams have been tabulated in the work at MPI. Information on the precipitation and evaporation averaged over land and sea is reproduced in Table1 below. ERA-40 results (based on six-hour forecasts) are compared with those from ERA-15 for Stream-1 and with those from the NCEP reanalysis for Stream-2 and Stream-3. Comparison is also made with the datasets of the GPCC (Global Precipitation Climatology Centre; Rudolf *et al.* (1996)), GPCP (Global Precipitation Climatology Project; Huffman *et al.* (1997)), CMAP (CPC Merged Analysis of Precipitation; Xie and Arkin (1997)) and CRU (Climate Research Unit; New *et al.* (2000)). For the two earlier periods only CRU data over land excluding Antarctica are available as observations. Also shown are climatological estimates (denoted BR) from Baumgartner and Reichel (1975).

The Stream-1 ERA-40 precipitation for the years 1989 to 1995 is substantially larger than given by any of the verifying datasets, and substantially larger than the ERA-15 precipitation for the years 1989 to 1993. Precipitation exceeds evaporation over sea as well as land. Stream-3 precipitation is also relatively high, though not as high as in Stream-1. Again, precipitation exceeds evaporation over sea as well as land. Only in Stream-2 (when no satellite data were available for assimilation) is the oceanic precipitation, averaged globally, of the order of that given in the observational datasets for the various periods, and less than the oceanic evaporation.

The ERA-15 precipitation exhibits global means similar to those of the verifying datasets, but this masks an underestimation in the extratropics and an overestimation in the tropics. The dry northern winter dry bias seen in ERA-15 does not exist in ERA-40. The ERA-40 assimilation system produces particularly high values of precipitation over the tropical oceans in the satellite era, especially after 1991. The smaller overestimation of precipitation over land indicated by Table 1 is also mainly located in the tropics, where it is similar to that of ERA-15.

3.2   Analysed tropical total-column water-vapour

The excessive tropical oceanic precipitation in the later years of ERA-40, particularly in Stream-1 after 1991, is the most serious problem diagnosed in the ERA-40 analyses to date. Maps of analysis increments and observing-system experiments have confirmed what might be inferred from the above results: that the Stream-1 analyses are generally moistened over tropical oceans by the assimilation of HIRS and SSMI data. Fig.11 presents time series of tropical-means of the increment in TCWV, the precipitation from 6-hour background

Stream-2: 1958-1961	ERA-40	NCEP	CRU	BR
Precipitation P over land	92	117	103	111
Evaporation E over land	71	96	-	71
Precipitation P over ocean	401	409	-	385
Evaporation E over ocean	472	453	-	424

Stream-3: 1973-1975	ERA-40	NCEP	CRU	BR
Precipitation P over land	123	117	103	111
Evaporation E over land	72	94	-	71
Precipitation P over ocean	454	384	-	385
Evaporation E over ocean	446	429	-	424

Stream-1: 1989-1995	ERA-40	ERA-15	GPCC	GPCP	CMAP	BR
Precipitation P over land	116	114	97	106	98	111
Evaporation E over land	76	83	-	-	-	71
Precipitation P over ocean	476	390	-	376	394	385
Evaporation E over ocean	448	434	-	-	-	424

Table 1: Global precipitation and evaporation over land and ocean for the years 1958-1961, 1973-1975 and 1989-1995 in $10^{15}kg/year$ from reanalyses and from the data sources listed in the text. The ERA-15 results are for the shorter Stream-1 period 1989-1993.

forecasts and the TCWV itself for Stream-1 from January 1989 to September 1998. A substantial jump in the precipitation rate can be seen over the second half of 1991. After a slight decline, the rate rises sharply again towards the end of 1994, with high rates (averaging around 5.5 mm/day) maintained throughout 1995 and 1996. This temporal variation in precipitation rate closely follows the temporal variation in the increment in TCWV, and the agreement between the red and the blue curves shown in the middle panel indicates that the moistening introduced by assimilating the HIRS and SSMI data is mostly rejected by the assimilating model, assuming an underlying precipitation rate of around 3.75 mm/day in the absence of humidity observations. Fig. 12 shows this to be a reasonable assumption. It presents Stream-2 results from January 1958 to June 1965, and shows only weak drying increments from the assimilation of *in-situ* tropical data. Precipitation rates are in the range 3.6 to 4.0 mm/day. Although most of the Stream-1 increment (which amounts to around a 1% increase in TCWV every six hours) is rained out (as it must be for the TCWV to keep reasonable values), the TCWV is nevertheless on average around 10% higher in Stream-1 than Stream-2, generally increasing over the period and reaching particularly high values during the strong 1998 El Nino event.

3.3 The use of HIRS infra-red radiances, and the influence of volcanic aerosol

The substantial increase in rainfall rates from the second half of 1991 onwards was due in part to effects of volcanic aerosols on HIRS infra-red radiances following the eruption of Mt. Pinatubo. The effects of aerosols were not included directly in the forward radiative transfer model used in the variational analysis. Instead they had to be absorbed into the bias corrections applied to the radiance measurements. This was a problem especially for data from the NOAA-12 satellite that became operational around the time Mt. Pinatubo erupted. Inadequately corrected infra-red radiance biases tend to result in humidity changes in the tropical troposphere, since the relatively low background errors in temperature force analysis changes to be predominantly in humidity. One

of a series of short data-impact experiments has shown that assimilating only radiance data from the so-called HIRS 'temperature' channel 5 gives a mean increment of 0.15 kg/m^2 in tropical-mean TCWV over the eight analysis cycles for 1-2 September 1995, about a third of the net increment of the production assimilation for this period. Moreover, NOAA-12 data from HIRS channel 10 were blacklisted from August 1994 onwards due to instrument drift seen in monitoring statistics. Until then, this channel had produced a drying tendency that countered the general moistening coming from other HIRS channels.

A further complicating factor in the study of Stream-1 results is an erroneous bias correction of SSMI data. This problem was present also in ECMWF operations from April 2000 to January 2002. It was remedied in ERA-40 analyses from January 1993 onwards.
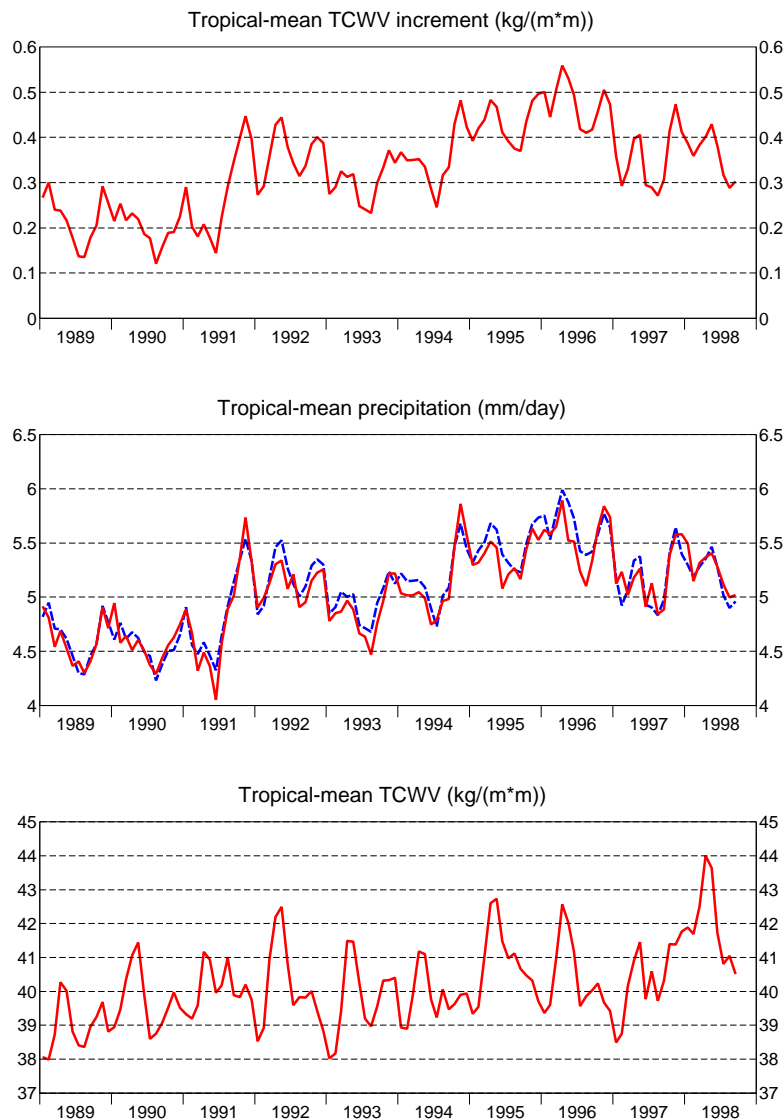

Figure 11: Tropical-mean increments in total-column water-vapour (kg/m^2, upper), precipitation rate from six-hour forecasts (mm/day, middle), and total-column water-vapour (kg/m^2, lower), averaged over all analysis cycles for each month of ERA-40 from January 1989 to September 1998. The blue dashed curve in the centre panel shows an estimate of precipitation based on assuming that the assimilating model would produce a precipitation of 3.75 mm/day in the absence of humidity observations, and that all humidity added in the tropics by the analysis system is rained out in the tropics within the same month.
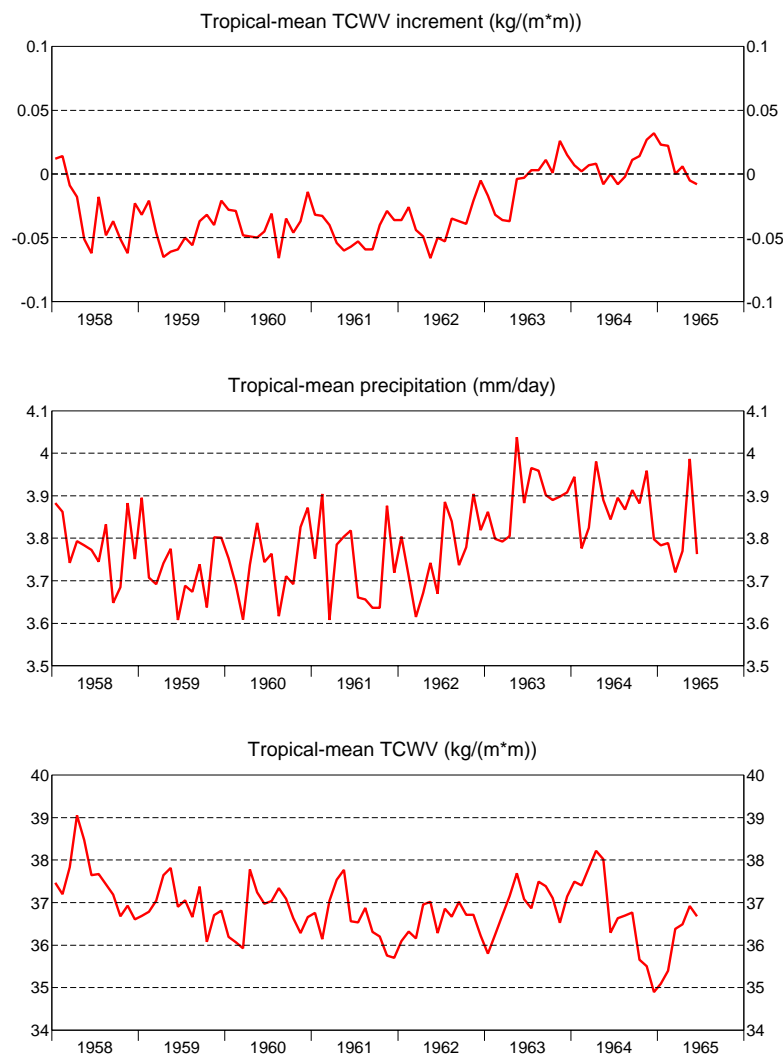
Figure 12: Tropical-mean increments in total-column water-vapour (kg/m^2, upper), precipitation rate from six-hour forecasts (mm/day, middle), and total-column water-vapour (kg/m^2, lower), averaged over all analysis cycles for each month of ERA-40 from January 1958 to June 1965.

A revised thinning, channel-selection and quality control of HIRS radiances has been developed and tested. The tropical-mean precipitation rate was reduced from 5.4 to 4.6 mm/day in the average for October 1995. This new treatment of HIRS data has been used for Stream-1 from January 1997 onwards, and will be used in Stream-3 when it has progressed to the time that HIRS data can be used. The change has also been shown to give slightly improved short-range forecast verifications, and it eliminates a further problem of concern in ERA-40: a cold bias in the lower troposphere (below about 500 hPa) over ice-covered oceans in both the Arctic and the Antarctic.

This change to the use of HIRS radiances, though clearly beneficial, by no means addresses completely the problem of high tropical precipitation in ERA-40. Average Stream-1 rainfall rates for 1997 and 1998 are lower than for 1995 and 1996, but are more than 10% higher than for 1989 and 1990, and more than 20% higher than for Stream-2. The green curve in Fig. 13 shows a tropical-mean precipitation rate as high as 5 mm/day for 1992 based on six-hour forecasts from 12 UTC analyses from an assimilation in which no HIRS radiance data was used. The figure also shows that rainfall rates from six-hour operational forecasts for more than the past five years are at least of the same order as those from the post-1991 ERA-40 forecasts. Difficulties with

the assimilation of the post-Pinatubo HIRS raw radiances may contribute to higher precipitation rates from ERA-40 than ERA-15 rates in 1992 and 1993, but ERA-40 rates were also higher than ERA-15 early in 1989. SSMI data were not assimilated in ERA-15.
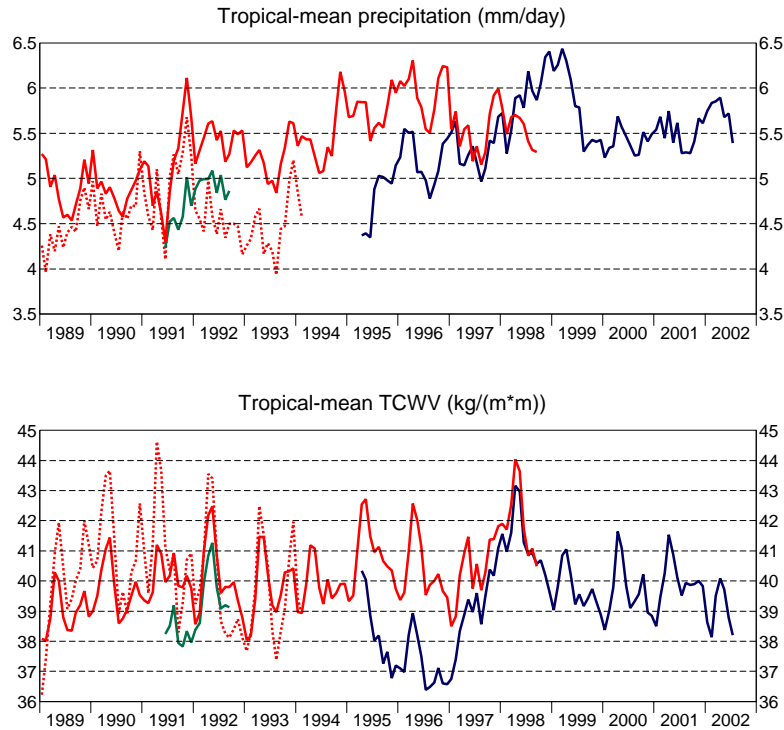

Figure 13: Tropical-mean precipitation rate from six-hour forecasts (*mm/day*, upper) and analysed total-column water-vapour (kg/m^2, lower). Averages of 12 UTC analyses and forecasts are shown for each month from January 1989 to July 2002. The solid and dotted red lines denote results from ERA-40 and ERA-15 respectively. The short green lines denote results using the ERA-40 system but with no assimilation of HIRS radiances. The blue lines denote results from ECMWF operations.

On a more encouraging note, there is considerable agreement as regards short-term (month-to-month) variability in precipitation rate and TCWV between the different analyses shown in Fig. 13. This is the case even between ERA-40 and operations for 1995 and 1996 when absolute values differ substantially.

3.4   Spin-up/spin-down characteristics in ERA-40 short-range forecasts

Forecasts to ten days ahead have been completed from all 00 UTC and 12 UTC ERA-40 analyses for selected years from each of the three streams. It is instructive to examine the spin-up/spin-down characteristics for each stream. Precipitation rates averaged over the whole globe, and averaged separately over land and over sea, are presented as functions of forecast range in Fig. 14. For the combined Stream-2 years of 1958 and 1959 (short dashed lines) precipitation spins up quite rapidly, increasing by more than 10% in the first two days of the forecasts, as the model counters the drying introduced by the assimilation of *in-situ* data. In contrast, for the Stream-3 and Stream-1 years of 1973 and 1996 respectively, there is an initial spin-up, followed by a spin-down out to about day 4. By this time, precipitation rates are similar for all years (apart from values over land for 1973) and thus indicative of the model's inherent rates.

It has been noted earlier that in the monthly mean, the ERA-40 assimilation system rains out about the same amount of moisture in its background forecasts as is added to the system by the analysis of HIRS and SSMI
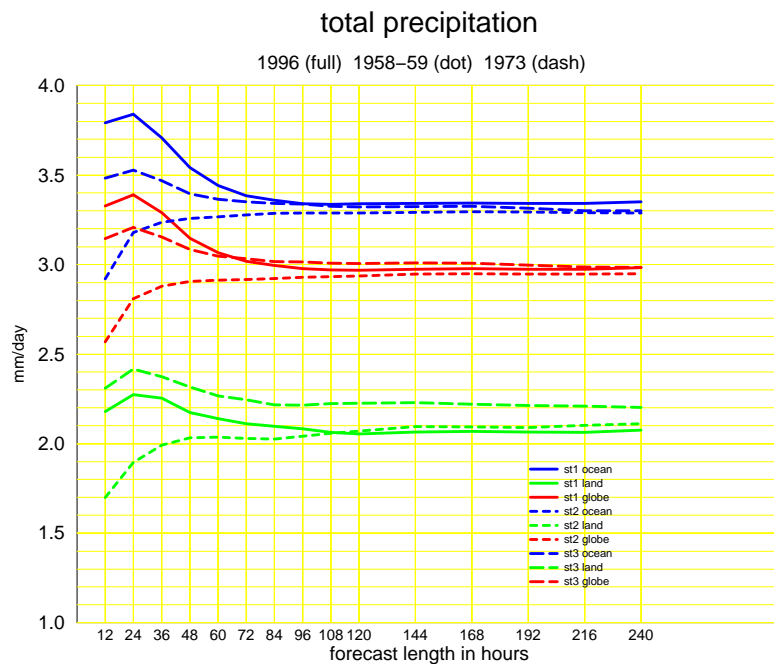
total precipitation

1996 (full) 1958–59 (dot) 1973 (dash)

Figure 14: Precipitation rate (*mm/day*) averaged over twice-daily ten-day forecasts carried out for 1996 (solid lines), 1973 (long dashed lines) and 1958/59 (short dashed lines). Means for either a 12-hour forecast interval (to day five) or a 24-hour forecast interval (from day five to day ten) are plotted. The red lines show global-mean values, and the blue and green lines show separate means for ocean- and land-surfaces respectively.

data. The spin-down characteristics show, however, that the timescale for the rain-out is longer than the six-hour interval between analyses. The assimilation system is designed to assimilate HIRS data only in cloud-free regions and SSMI data in rain-free regions. The humidity analysis thus tends to moisten away from regions of strong, precipitating ascent, and there is a time lag between the addition of moisture by the analysis and the subsequent rain-out of that moisture.

3.5   Discussion

Various deficiencies of the assimilation system have been suggested as causes of the large tropical rainfall rates seen in the short-range ERA-40 and operational forecasts. Problems with the bias-correction of the satellite radiances, the vertical structure of the increments produced by the analysis scheme and the model representation of tropical moist processes are all possible candidates, and some sensitivity has been seen to changes in these areas. However, excessive tropical precipitation is a feature that has survived many changes to the forecasting system, and others have experienced difficulties in introducing assimilation of TCWV retrievals from SSMI data. The problem thus appears to be a quite general one. If tropical circulations in assimilation cycles are too intense, there will be a tendency for descent regions to be too dry. It is in just these regions that the satellite humidity data tend to be used, and the observations act to correct what they see to be a too-dry atmosphere. The moisture added in the descent regions may then be fed into the precipitating ascent regions, where it can fuel the maintenance of the too-strong circulations. If this is indeed a significant factor, then part of the solution lies in the development of a multivariate analysis in which a mismatch between observed and background humidity implies an accompanying adjustment of the vertical velocity (as may happen to some degree in 4D- rather than 3D-Var), while assimilation of rain-affected microwave radiances would offer a further control.

The difficulties discussed here provide a major motivation for rerunning the latter part of ERA-40. The extent

of the improvement that can be achieved before the rerun is not yet clear, but the main variations in precipitation arising from direct Pinatubo-aerosol effects on HIRS radiances and from the changes made to the use of SSMI and HIRS radiances will at least be removed.

4   Satellite remote-sensing of humidity

In recent years, NWP centres have shown the benefit of assimilating water-vapour information from satellites into numerical models. For example, McNally and Vesperini (1996) have clearly shown that the assimilation of TOVS radiances using 1D-Var successfully improved some aspects of the hydrological cycle of the ECMWF system. Moreover, they found that the forecasts could retain a memory of humidity changes for up to 5 days. More recently, Gérard and Saunders (1999) demonstrated that the assimilation of TCWV data from SSMI could reduce model biases, especially in very dry areas.

Due to the scarcity of conventional upper-air data to constrain the model humidity fields over the oceans, satellite data indeed offer a valuable source of information that is being exploited at ECMWF. It should be added that the move from using retrievals to direct radiance assimilation in 3D-Var (Andersson *et al.* (1994), McNally *et al.* (1999)) as well as the implementation of 4D-Var (Rabier *et al.* (2000)) have allowed a continuous improvement in the assimilation of information from satellite instruments (Simmons and Hollingsworth (2002)).

4.1   Currently available humidity-sensing satellite instruments

Today, several humidity sensitive satellite observations are available for monitoring or assimilation in the ECMWF assimilation system:

- *HIRS radiances from NOAA-14, 15, 16 and 17 satellites, in particular channels 12 (6 micron) and 11 (8 micron).* Currently, all these radiances are monitored, but only HIRS channel 12 from NOAA 14 is actively assimilated. This observation source thus essentially constrains the model upper-tropospheric humidity.

- *AMSU-B radiances from NOAA-15, 16 and 17 satellites.* These data are routinely monitored. Although the noise characteristics for the AMSU-B instrument are fairly poor, several NWP centres have been successful in assimilating this information (e.g. English *et al.* (2002)). It is planned to assimilate data from this instrument also at ECMWF, in the near future.

- *Water vapour radiances (6 micron) from the geostationary satellites METEOSAT-5 and 7, GOES-8 and 10.* Clear-sky radiances from METEOSAT-7 are operationally assimilated, with GOES data used in pre-operational tests. The other geostationary satellites are currently monitored with plans for operational assimilation in the near future.

- *SSMI radiances from DMSP-13, 14 and 15 satellites.* These radiances are currently assimilated in the ECMWF system indirectly through a 1D-Var retrieval approach that produces TCWV and surface wind speed information for subsequently assimilation in the 4D-Var system. Preparations have been made to replace the 1D-Var approach by direct assimilation of SSMI radiances. Data from DMSP-13 and 14 is assimilated operationally at present. The addition of DMSP-16 is planned for the autumn 2002.

The main shortcoming of the current instruments is their poor vertical resolution, which makes the distribution of humidity information in the vertical a delicate problem. Fig.15 displays the humidity Jacobians ($\partial Rad/\partial q$) of

the above-mentioned instruments. The broadness of the Jacobians (similar to weighting functions) indicate that these data contain very little information about the vertical structure of humidity, and are therefore ineffective in analysing sharp features such as the boundary layer top and the tropopause. The distribution of humidity increments in the vertical then relies on the background-error covariance. It is hoped however that the new generation of sounding instruments such as AIRS and IASI on board AQUA and METOP, respectively, will substantially improve the vertical description of atmospheric moisture, although it is doubtful that they will be able to resolve the boundary layer top. Further improvements are expected with passive limb instruments and GPS radio-occultation measurements, which will provide very high vertical resolution measurements.
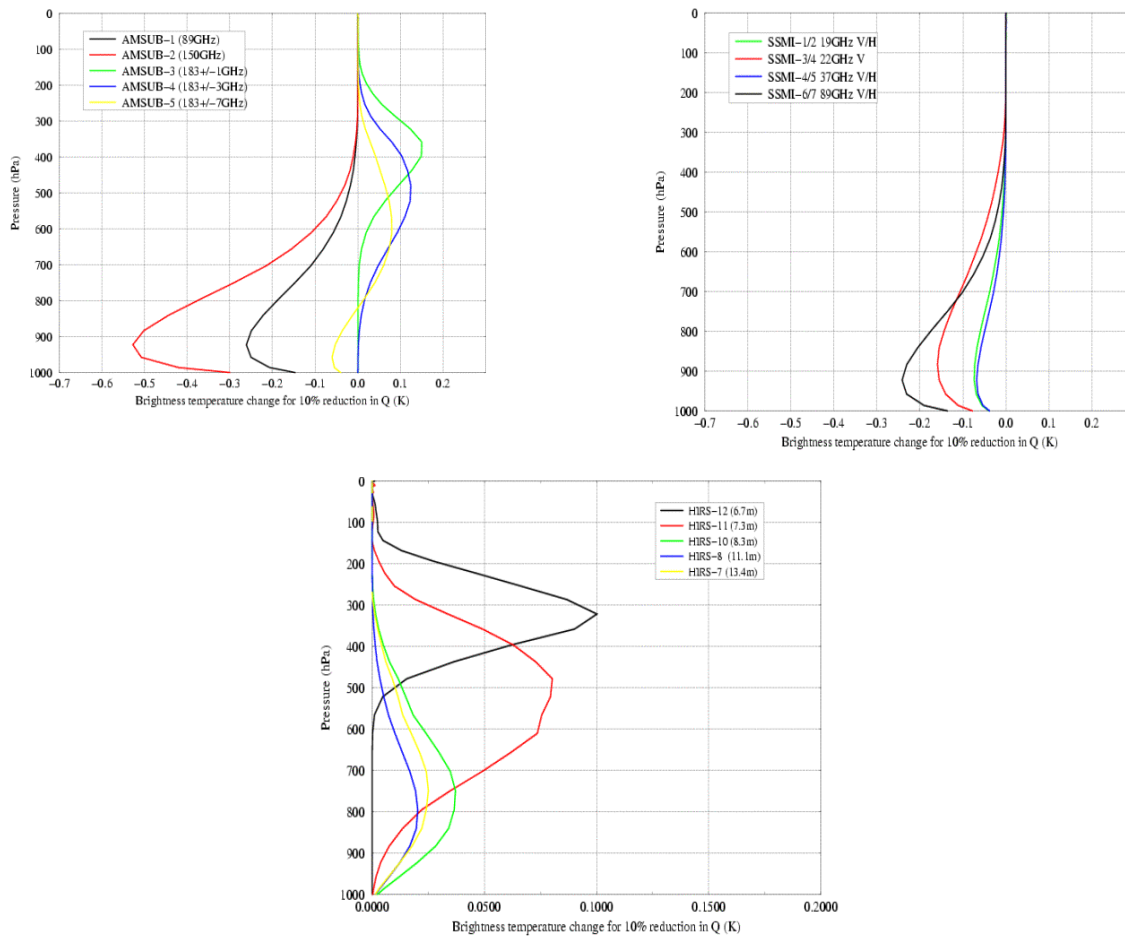

Figure 15: Jacobians ($\partial Rad/\partial q$) for AMSU-B (top left panel), SSMI (top right panel) and HIRS water-vapour channels (lower panel) corresponding to a 10% change in a specific humidity profile.

Another important aspect of the assimilation of humidity-sensitive radiances concerns the quality of the radiative transfer (RT) model. Indeed, the direct assimilation of radiances has been preferred because of a better consistency between different satellite observations and an easier description of observational errors in radiance space. However, great care has to be taken to handle properly systematic errors in the observations and in the radiative transfer model.

4.2 Improvements of the radiative transfer modelling for water vapour

An improved version of the RTTOV fast regression-based radiative transfer model has been developed by Matricardi *et al.* (2001). This new model computes radiances for the AIRS instrument as well as current NOAA instruments. The main deficiencies that had been identified in RTTOV-5 (the version used at ECMWF until January 2002) concerned the ability of the fast model to reproduce line-by-line simulations for the surface-sensing, the ozone channel and more importantly for the water-vapour channels. Also significant differences between water-vapour Jacobians from RTTOV-5 and line-by-line models had been identified (Garand *et al.* (2001)). A revised set of regression predictors was introduced for ozone and new predictors were added to model the water vapour continuum absorption. Furthermore, improvement of the water-vapour Jacobians was achieved by weighting the data prior to performing the regression, thus avoiding the use of a split algorithm (split between optically thin and optically thick regimes).

As noted in Matricardi *et al.* (2001), the improvement of the new version in terms of fit to line-by-line simulations can be as large as a factor of seven for the 6-micron water-vapour channels. To validate the performance of the new model, two twin assimilations have been run for three weeks from 20001112 to 20000512. The assimilation system used is a 3D-Var system similar to the ERA-40 reanalysis configuration. The control assimilation used RTTOV-5. The model first-guesses from the control experiment were then used together with the new RTTOV model to compute new observation departure statistics from which new satellite bias corrections were obtained. The trial experiment is identical to the control apart from the use of the new RTTOV version and the new bias correction files in the assimilation suite. Fig. 16 presents the NOAA-14 HIRS-11 and HIRS-12 scan bias corrections used in the control experiment (left panel) and in the trial experiment (right panel). One can clearly see a decrease of the scan bias, especially in the extra-tropics (dashed and dotted curves) in the trial assimilation. Fig. 17 presents the mean departure between uncorrected NOAA-14 HIRS-11 and 12 radiances and the model (solid curve), between bias-corrected NOAA-14 HIRS-11 and 12 radiances and the model (dotted curve) as well as plus/minus one standard deviation of the corrected departure (dashed curve). These departures are plotted as a function of time. The left panel shows the control experiment and the right panel shows the trial. The curves for the uncorrected data show an improvement of the fit of the model to HIRS-11 and 12 radiances by 0.2 to 0.3 K in the trial experiment, indicating a better general description of the upper-tropospheric humidity in the assimilation. In particular, the comparison to HIRS-11 (which is monitored but not used actively in both experiments) is particularly encouraging. Forecast scores accumulated over the three week period are near-neutral (not shown).

These improved features of the RT-model were implemented operationally at ECMWF in January 2002 and are also part of the new RTTOV-7 package that has been delivered by the NWP-SAF to the user community. This new version is an essential step towards accurate assimilation of water-vapour channels also from MSG (METEOSAT Second Generation), AIRS and IASI.

4.3 Direct assimilation of water-vapour radiances from METEOSAT

Clear-sky water-vapour radiances (6.3 micron) from the METEOSAT geostationary satellites are sensitive to the upper-tropospheric humidity. Similarly to HIRS-12 on board NOAA satellites, the weighting function of this channel is very broad and provides no information on the vertical distribution of humidity. As stated above, the clear-sky water-vapour radiances from the METEOSAT satellites have been routinely monitored at ECMWF for a number of years. More recently, it has been shown (Andersson *et al.* (2002)) that 4D-Var can indeed exploit the temporal information in high time-frequency data very effectively (e.g. hourly surface-pressure data, wind-profiler data and also geostationary radiances). The direct assimilation of water-vapour radiances could provide an alternative to, or complement, the assimilation of water-vapour winds with their
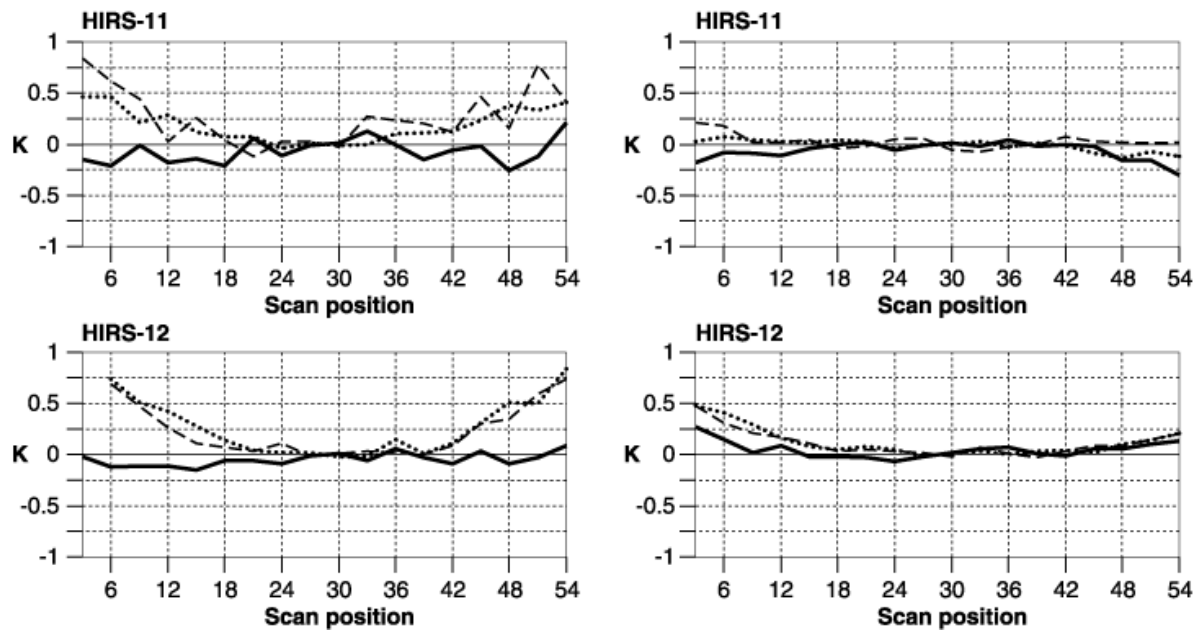
Figure 16: Scan bias correction for the channels HIRS-11 (top) and HIRS-12 (lower panels) of NOAA-14 for the control experiment (left panels) and the trial experiment (right panels) testing the impact of the modified RTTOV radiative transfer model (see main text for a full description). The solid curve denotes tropics, the dashed curve 50 ^oS and the dotted curve $45^oN - 75^oN$.
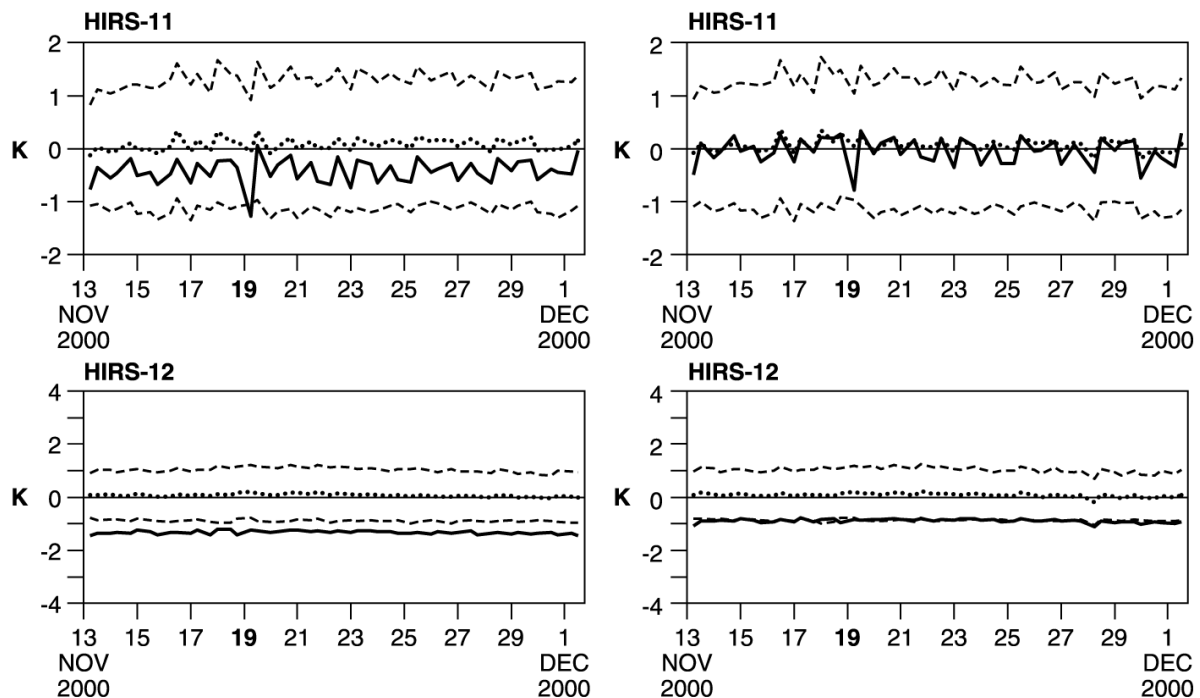

Figure 17: Mean value of the difference between measured and modelled radiances for channels HIRS-11 and 12 of NOAA-14 for the CONTROL (left panel) and RTTOV_new experiment (right panel). The solid curve denotes the uncorrected departure, the dotted curve the departure after bias correction and the dashed curves show plus/minus one standard deviation of the bias corrected departure.

problematic height assignment. By capturing the time evolution of upper-tropospheric humidity, 4D-Var will not only exploit the observational information on humidity but also on the dynamics that drive the atmospheric moisture. These arguments have motivated attempts to assimilate directly the clear-sky water-vapour radiances in the ECMWF 4D-Var system. A full description of the monitoring and the assimilation experiments using METEOSAT radiances in 4D-Var is given in Köpken et al. (2002).

The reported radiance data from METEOSAT represent averages over those pixels within a 16×16 pixel 'quadrant' that are diagnosed (by the data producers) as cloud free, corresponding roughly to a resolution of $80 \times 80 \, km^2$. Since 29 May 2000, a calibration based on its onboard blackbody has been implemented for METEOSAT-7 and has resulted in considerably more stable radiance monitoring statistics — a prerequisite for successful assimilation of the data.

Routine time series show that METEOSAT-7 observations are on average 3.5 K to 4.0 K warmer than the brightness temperatures calculated from the model profiles. Therefore, prior to the assimilation, a bias correction scheme is applied to the radiance data. The bias correction used for the METEOSAT radiances follows the statistical regression method applied for other radiance data (Harris and Kelly (2001)), with the exception that skin temperature has been excluded from the predictors, as the water-vapour channel is insensitive to the surface and the lower troposphere.

Hourly monitoring statistics show regular spikes caused by solar stray light intruding into the telescope around local midnight. This effect is particularly intense close to the eclipse seasons where bowed bands or bright spots can be visible on the water-vapour image. As described in Köpken (2001), a safe blacklisting strategy excluding time slots around local midnight from several weeks before until several weeks after the eclipse seasons, has been implemented.

With the two elements mentioned above (bias correction and careful quality control in particular close to the eclipse season), assimilation experiments using METEOSAT-7 radiance data have been performed, followed by operational implementation in April 2002. Results from the assimilation experiments include:

- A mean impact on the moisture field is seen in areas of known model deficiencies, e.g. a high-level drying of the inner ITCZ area where convection in the model tends to be too persistent.

- While the fit to conventional data remains unchanged, the fit to other independent water-vapour radiances is improved. This is illustrated in Fig. 18, which shows time series of monitoring statistics for HIRS-12 on NOAA-16 from the experimental suite (including the active assimilation of METEOSAT-7) for the period 21 February to 4 April 2002. The statistics for HIRS-12 data are from a square area covering the METEOSAT-7 disk. The top panel shows mean differences OBS minus FG and OBS minus AN and the bias corrected values. The bottom panel shows standard deviations of the observations (blue) and the mean departures: OBS-FG (green) and OBS-AN (red). From 4 to 26 March, METEOSAT-7 assimilation was switched off to allow a retuning of the bias correction following a sudden 0.5 K jump in the METEOSAT-7 bias on the 26 February. One clearly sees a degradation of the model FG fit to HIRS-12 on NOAA 16 when METEOSAT-7 data were taken out, confirming the positive impact of METEOSAT-7 data.

- The assimilation of hourly geostationary radiances leads to increments in the wind field. Comparisons versus conventional observations show a slightly improved fit to tropical PILOT data. This confirms the ability of 4D-Var to use high time frequency humidity information in a dynamically consistent way.

- A small but statistically significant positive forecast impact was found for upper level geopotential and winds in some areas, while the forecast impact is neutral elsewhere.

Current work is focussing on improving the quality control of the clear-sky water-vapour radiance data, increasing the horizontal coverage of upper-tropospheric humidity information by including the new GOES imager data and also METEOSAT-5 (over the Indian Ocean) into active assimilation, and preparing the system for the use of MSG radiances.
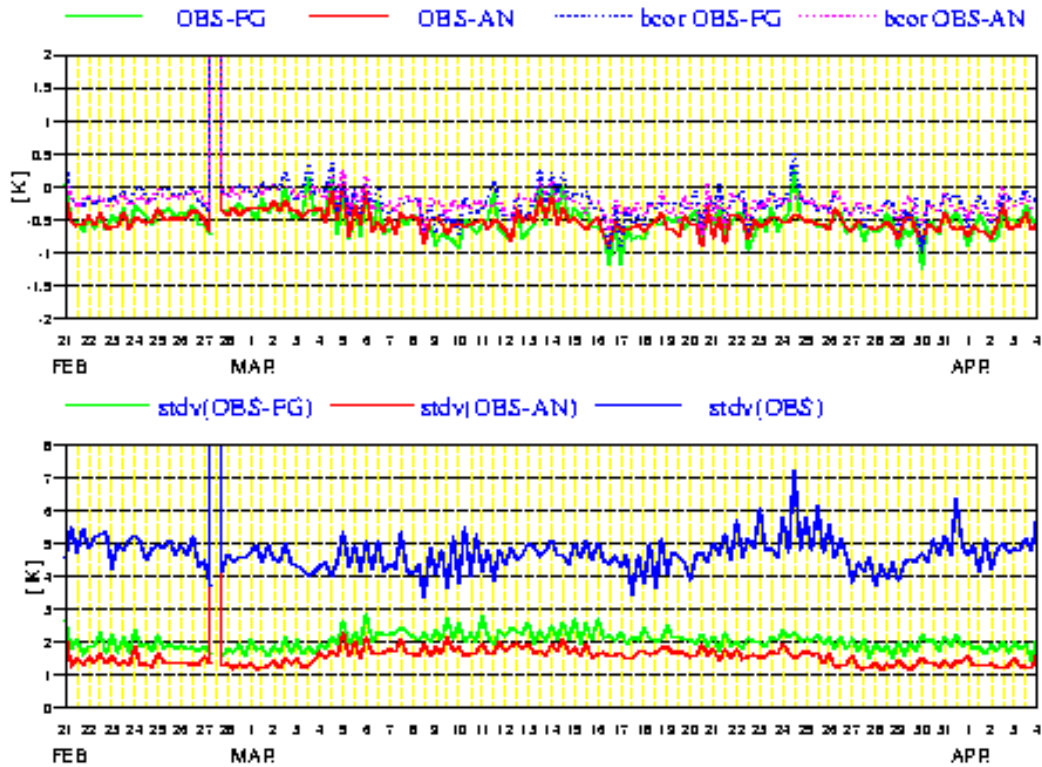

Figure 18: Time series of monitoring statistics for HIRS-12 on NOAA-16 from the experimental suite (including the active assimilation of METEOSAT-7) for the period 21 February to 4 April 2002. The statistics are from a square covering the METEOSAT-7 disk. The top panel shows mean differences OBS minus FG and OBS minus AN and the bias corrected values. The bottom panel shows standard deviations of OBS (blue) and mean departures OBS-FG (green) and OBS-AN (red).

4.4 Assimilation of SSMI total-column water-vapour data in clear and cloudy regions

The Special Sensor Microwave Imager (SSMI) instruments on board DMSP-13, 14 and 15 measure horizontally and vertically polarized radiation at three frequencies (19, 37 and 85 GHz) and vertically polarized radiation at 22 GHz. Because these essentially window channels are differentially affected by water vapour absorption, they provide information on TCWV. In addition, the strong dependence of the sea surface emission on surface roughness allows the extraction of surface wind speed information from SSMI channels.

4.4.1 Current use of SSMI data in the assimilation system

Radiances from SSMI are supplied to a one-dimensional variational analysis scheme (1D-Var) (Phallipou (1996)). The 1D-Var approach adjusts model TCWV and wind speed by fitting the model radiances (using a fast radiative transfer model RTSSMI described in Phallipou (1993)) to the observed ones. This approach is

optimal only in one dimension in that it takes into account the background, radiative transfer and observations error covariances for one column at a time. The 1D-Var adjusted TCWV and wind speed are then supplied as retrieved products to the operational 4D-Var assimilation system.

The largest analysis changes caused by the assimilation of SSMI TCWV information occur in the tropics and the Southern Hemisphere. Here data cause a significant moistening of the analysis, which is difficult to verify due to the absence of any extensive conventional observing system measuring TCWV. However, earlier studies such as McNally and Vesperini (1996) have shown a good agreement between TCWV from SSMI and the humidity information from other satellite instruments such as HIRS on board NOAA satellites. This and other validation studies give confidence in the use of SSMI humidity information to reduce model biases.

The humidity analysis changes in the tropics by the SSMI TCWV information are retained by the forecast for only about 3 days, as the extra humidity introduced by SSMI is removed by precipitation. Humidity changes in the Southern Hemisphere extra-tropics, however, can persist out to day 5 in the forecast. Otherwise, assimilation experiments including SSMI TCWV indicate a neutral to slightly positive impact in terms of the standard geopotential and wind hemispheric scores (not shown).

4.4.2 SSMI direct radiance assimilation

Since the operational implementation of 3D-Var in 1996 the direct assimilation of radiances has been preferred, rather than the use of retrievals, as radiance assimilation more accurately accounts for the actual information content in the data. To improve the consistency of treatment between SSMI and other microwave satellite instruments, the current SSMI 1D-Var framework is being replaced by direct assimilation of SSMI radiances in the 4D-Var system. The same radiative transfer model (RTTOV) is then used for all satellite instruments. However, for SSMI an updated parametric surface emissivity model (and its adjoint) was required, to account for its wind speed dependence. For this purpose FASTEM-2 (English and Hewison (1998)) has been implemented in the new version of RTTOV with a significantly increased accuracy and computational efficiency with respect to the emissivity model in RTSSMI. A further difference between the two approaches is that the 1D-Var in addition retrieves cloud liquid water path and therefore avoids the danger of aliasing cloud effects into retrieved TCWV and wind speed. A similar treatment of clouds is not yet in place in the direct radiance assimilation framework. Therefore, a tighter cloud screening is applied to remove cloud affected radiances.

Several weeks of parallel assimilation comparing the two approaches have been performed. The new route using RTTOV, and assimilating the radiances directly, exhibits much better OBS-FG statistics: smaller first-guess departures and narrower distribution (not shown). The impact in terms of forecast scores is marginally positive.

4.5 Humidity information expected from future satellite missions

A number of instruments on board new and planned satellite missions will further enhance the observational capabilities of the highly variable distribution of humidity in the atmosphere:

- The SEVIRI instrument on board METEOSAT Second Generation (MSG) will have four times as many channels as the current METEOSAT instruments. Extra window channels will certainly improve the cloud detection and the subsequent quality indicator of the MSG clear-sky radiances. More importantly, two water-vapour channels (7.3 and 6.2 micron) will be available, modestly increasing the vertical resolution.

- The SSMI/S on board DMSP-16 combines AMSU-A, AMSU-B and SSMI sensing capabilities in a single instrument. The combined availability of imaging and sounding channels will improve the vertical resolution with respect to water vapour structures. While the imaging channels are predominantly sensitive only to TCWV, the channels around 183 GHz will resolve the middle-tropospheric water-vapour profiles with the same viewing geometry and similar foot print resolution as the imaging channels. The additional temperature sounding channels will further constrain the inversion of the radiance information into water vapour and temperature in the assimilation.

- AIRS on board AQUA (successfully launched in June 2002) and IASI on board METOP (expected launch in 2005) provide a substantial increase of water-vapour information compared with the current infra-red radiometers. An example is given in Fig. 19, which shows the water-vapour averaging kernels for HIRS (left panel) and AIRS (right panel) for the 43 vertical levels of the current version of RTTOV. Averaging kernels (Rodgers (2000)) describe how in a 1D-Var context, the retrieved water-vapour profiles respond to a fractional change in water vapour at a given level. They take into account not only the weighting functions of the instrument but also the structure of the background-error covariance matrix, and as such provide a better indication of the actual vertical resolution of the water vapour retrieval than would the Jacobians alone do. Ideal kernels would display delta functions at each of the 43 RTTOV levels. It is clear from the figures that AIRS will substantially increase the vertical description of moisture. Assimilation experiments with real AIRS data will tell if this class of high-spectral resolution instruments will provide enough vertical resolution to constrain the boundary layer top and the tropopause height, in the assimilation.

- Passive limb sounders (such as MIPAS on board ENVISAT) and active GPS radio-occultation measurements (GRAS, ACE+ and other planned missions) will provide very high vertical resolution measurements of water vapour. These new and planned missions are very promising, but also challenging, since they raise difficult assimilation problems in the horizontal.
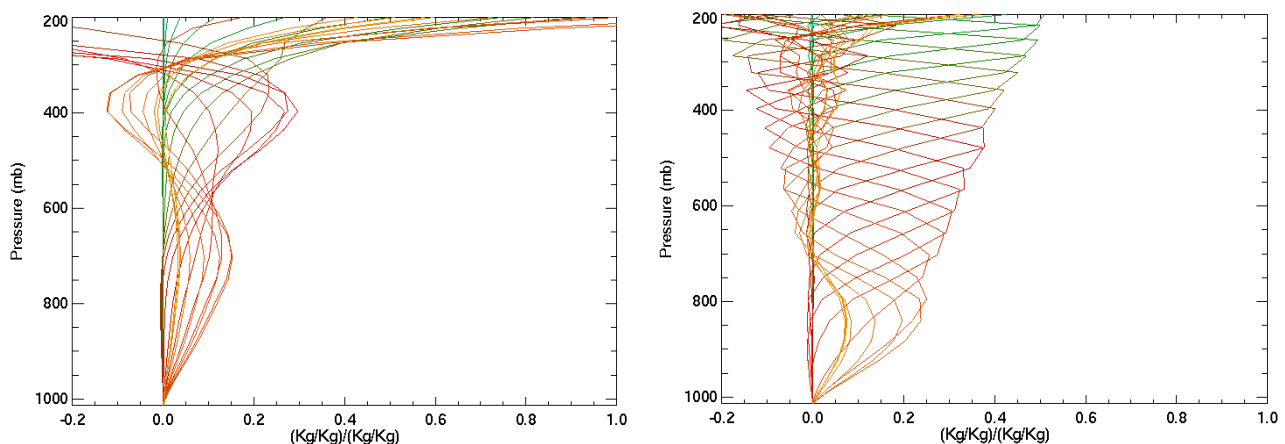

Figure 19: Water vapour averaging kernels (Rodgers (2000)) for HIRS (left panel) and AIRS (right panel) with respect to the 43 RTTOV pressure levels.

5 Cloud and rain assimilation

Operational NWP centres have a growing interest in assimilating satellite observations in cloudy and rainy regions (Treadon (1997), Macpherson (2001), Marécal and Mahfouf (2002b), Fillion and Mahfouf (2002),

Hou *et al.* (2001)). As clouds have a significant impact on the radiative and hydrological budgets of the atmosphere, measurements in cloudy regions contain valuable information on temperature, humidity and wind that is fundamentally different from those in clear-sky areas. Current satellites already provide some cloud-system information that is not generally assimilated in operational analyses. Using active sensors, a new generation of satellites will provide more precise measurements on clouds and precipitation — including their vertical distribution.

Variational assimilation schemes can in principle handle cloud and precipitation observations. However, these data represent features and processes that are more discontinuous and have smaller spatial and temporal scales than most currently used data. Therefore the accuracy and efficiency of the data assimilation systems will need to be improved.

Four approaches for cloud and rain assimilation have been defined:

- In Method-1, linearized parametrizations of moist physical processes (deep convection and large-scale condensation) are used in 1D-Var to find adjusted temperature and humidity profiles that produce rainfall in better agreement with observations. Retrieved TCWV is computed from the adjusted humidity profiles (Marécal and Mahfouf (2000)), for assimilation in 4D-Var, in rainy areas (Marécal and Mahfouf (2002a)).

- In Method-2, observations of rainfall rate are assimilated in 4D-Var, using linearized parametrizations of moist physical processes (and their adjoints) as observation operators (Marécal and Mahfouf (2002b)). See also Tsuyuki (1997).

- In Method-3, cloud and rain affected radiances are used in 1D-Var, with a radiative transfer model that includes cloud and scattering effects, to find adjusted temperature and humidity profiles that produce model radiances in better agreement with observations. Retrieved TCWV is computed from the adjusted humidity profiles for assimilation in 4D-Var (as in Method-1). Cloud parameter inputs to the RT-model in 1D-Var are obtained using a modified convection scheme (see below).

- In Method-4, cloud and rain affected radiances are assimilated directly in 4D-Var, using radiative transfer models that include cloud- and scattering effects, as observation operators. Cloud parameter inputs to the RT-model are obtained in 4D-Var from the moist physics of the forecast model, in its non-linear, linearized and adjoint versions.

Methods 1, 2 and 3 have been developed, and initial experimentation has been carried out. Method-4 is under development. These four methods are discussed in more detail in the following four subsections, respectively.

5.1   Assimilation of retrieved total-column water vapour in rainy areas

The launch of the Tropical Rainfall Measuring Mission (TRMM, Simpson *et al.* (1996), Kummerow *et al.* (1999)) in November 1997 led to the initiation of a 3-year EU-funded project (EuroTRMM) at ECMWF, on the assimilation of rainfall rates in the 4D-Var system.

Using Method-1, instantaneous rainfall rates derived from the TRMM Microwave Imager (TMI) at high spatial resolution (between 7 and 30 km) were first averaged at model resolution and compared to model counterparts within a 1D-Var assimilation. Results have shown that the 1D-Var is generally capable of finding modified profiles of temperature and humidity (within the range of typical background errors) that provide precipitation amounts closer to those observed (Marécal and Mahfouf (2000)). Increments of temperature are small indicating that the 1D-Var essentially adjusts humidity to achieve modified precipitation amounts. The 4D-Var

assimilation of TCWV in rainy areas has demonstrated a positive impact on the humidity analysis within the tropical belt (Marécal and Mahfouf (2002a)). The model rainrates at the analysis time are closer to the TRMM observations. The 4D-Var allows modifications on the humidity field to have a significant influence on the dynamics of tropical cyclones in terms of improved cyclone track in the analysis and deeper central pressure. The impact on the forecasts is a slight reduction of the precipitation spin-down over the tropical oceans. Objective scores for the tropics are improved, particularly for the wind and the upper-tropospheric temperature, despite the small number of observations (around 1000) introduced at each assimilation cycle. As the ECMWF model has a tendency to produce too much precipitation in the analysis, the main benefit of TRMM in the tropics comes from the no-rain information that results in a systematic beneficial drying of the tropical atmosphere. Given the strong sensitivity of the moist convection scheme to small changes in humidity in the boundary layer (Fillion and Mahfouf (2000)) and the relatively large horizontal scales of the background errors for humidity, it is likely that some clear-sky TCWV information provided by SSMI influence nearby cloudy and rainy regions. We have speculated in Section 3 that this could be an important contributing factor to the excessive tropical rainfall in ERA-40 and in the current operational system. Experiments show that the complementary use of TCWV in rainy areas is capable of reducing this detrimental effect.

As there can be large discrepancies between rainrate retrieval algorithms, the impact of using different TMI retrievals in 4D-Var was tested (Marécal *et al.* (2002a)). Even though the global impact on analyses and forecasts was almost unchanged, differences between three TMI products and their associated errors lead to significant changes in active systems (fronts, tropical cyclones). A better specification of retrieval errors was obtained (Bauer *et al.* (2002)) by accounting for horizontal correlations when upscaling rainrates from the satellite pixel resolution to the model resolution.

5.2   4D-Var assimilation of satellite-derived rainfall rates

Using Method-2, some inconsistencies in the current incremental formulation of the ECMWF 4D-Var (particularly inconsistencies between the models used in the inner and outer loops) were identified, which can prevent the minimization from converging (Marécal and Mahfouf (2002b)). Also the necessity to reformulate the coupling between the physics and the spatial interpolation operators in 4D-Var was demonstrated. The large values of rainfall Jacobians near the surface from the ECMWF moist convective parametrizations are partly responsible for the minimization failures. It was found that the background error covariance matrix needs modifications in rainy areas since the horizontal scales are currently too large (being representative of all-sky conditions). By comparing Method-1 and Method-2 it was found that the convergence of 4D-Var performs better with Method-1, but more important changes to the dynamical fields take place with Method-2. The impact of using SSMI rainrate retrievals instead of TMI retrievals is currently under study. Satellite derived rainrates from SSMI are less accurate than TMI in the tropics but they have a better spatial coverage, especially as there are currently three polar-orbiting operational DMSP satellites.

5.3   Use of rain-affected radiances in 1D-Var to retrieve total-column water-vapour, for assimilation in 4D-Var

In Method-3, multi-channel microwave brightness temperatures as measured by the satellite radiometer are used in 1D-Var. The method is otherwise similar to Method-1, in that the interface with 4D-Var is via retrieved TCWV. Since microwave brightness temperatures exhibit rather different sensitivities to cloud liquid water, ice, rain, water vapour and temperature in the various channels available, it is usually possible to extract useful information about each of these meteorological parameters. Method-3 requires a radiative transfer model that allows computation of the equivalent of the measured radiances from the forecast model state, even in rainy

conditions. Such a radiative transfer model has been developed at ECMWF by Bauer (2002) and its adjoint version is now available.

A comparison between Method-1 and Method-3 is shown in Fig. 20, for the case of supertyphoon Mitag close to the Philippines, at 5 March 2002 1200 UTC. In these experiments the modified convection scheme (next subsection) was used in 1D-Var, to produce the required cloud-parameter inputs to the RT-model. The figure illustrates that the analyzed rainfall rates are much closer to the observations with Method-3 than with Method-1. In particular, it should be noted that with Method-1 it is not possible to generate temperature and specific humidity increments wherever it is not raining in the model background; that is wherever the Jacobian of the model surface rainfall is zero. This limitation was also pointed out by Marécal and Mahfouf (2002b). On the contrary, Method-3 offers the possibility of correcting the model state even in non-rainy areas, and in particular to generate rain at dry places of the background through changes in the water-vapour field. This capability is due to the various sensitivities of the multi-channel microwave brightness temperatures. An additional advantage of Method-3 lies in the fact that the specification of observation error statistics is much easier for radiances than it is for rainfall retrievals. Its main drawback lies in the computational overhead required to run the radiative transfer model.

These advantages make the assimilation of radiances (Methods 3 and 4) more promising than the assimilation of rainfall rate retrievals (Methods 1 and 2). Method-3 will be preferred to Method-4 as long as some potentially problematic inconsistencies between the inner and outer loops (resolution, field representation, physical parametrizations) remain (see below).

5.4 Further developments in preparation for direct assimilation of cloud and rain-affected radiances

A central aspect of the assimilation of clouds and rain is the linearized physical processes that are necessary both for the time propagation of the analysis increments (and the gradient of the cost function) and to produce the sensitivity of the model counterparts to observations (adjoint of an observation operator). In addition to a modified convection scheme, the assimilation of cloud and rain also needs a cloud scheme (and its linearized versions) that can describe physically the generation of liquid water and rain in stratiform clouds. These are on-going developments that could lead to a consistent assimilation of SSMI brightness temperatures (at frequencies sensitive to liquid water only) in clear-sky and cloudy conditions. Comparisons have started between Jacobians of various cloud schemes in order to provide guidance for possible simplifications for a linearized scheme (Fillion and Mahfouf, 2002).

5.4.1 A modified convection scheme suitable for the assimilation of cloud and precipitation

A modified version of the operational ECMWF convection scheme (Tiedtke (1989)) has been developed for the purpose of the assimilation of space based precipitation data (e.g. SSMI, TRMM, GPM,…) in ECMWF's 4D-Var system. The main aim was to reduce the high degree of complexity of the operational mass-flux scheme in order to obtain a parametrization less subject to strong non-linearities, and thus more suitable for adjoint coding and 4D-Var assimilation. At the same time, this modified parametrization was designed to involve many fewer simplifying assumptions than the one currently used in the tangent linear and adjoint calculations of the 4D-Var inner loop.

In this modified scheme, all types of convection (shallow, mid-level, and deep) are now treated in a similar way, with in particular a common closure based on CAPE relaxation. The uncoupling of the equations for the updraft/downdraft mass-flux and thermodynamical variables circumvents the iterative procedure implemented
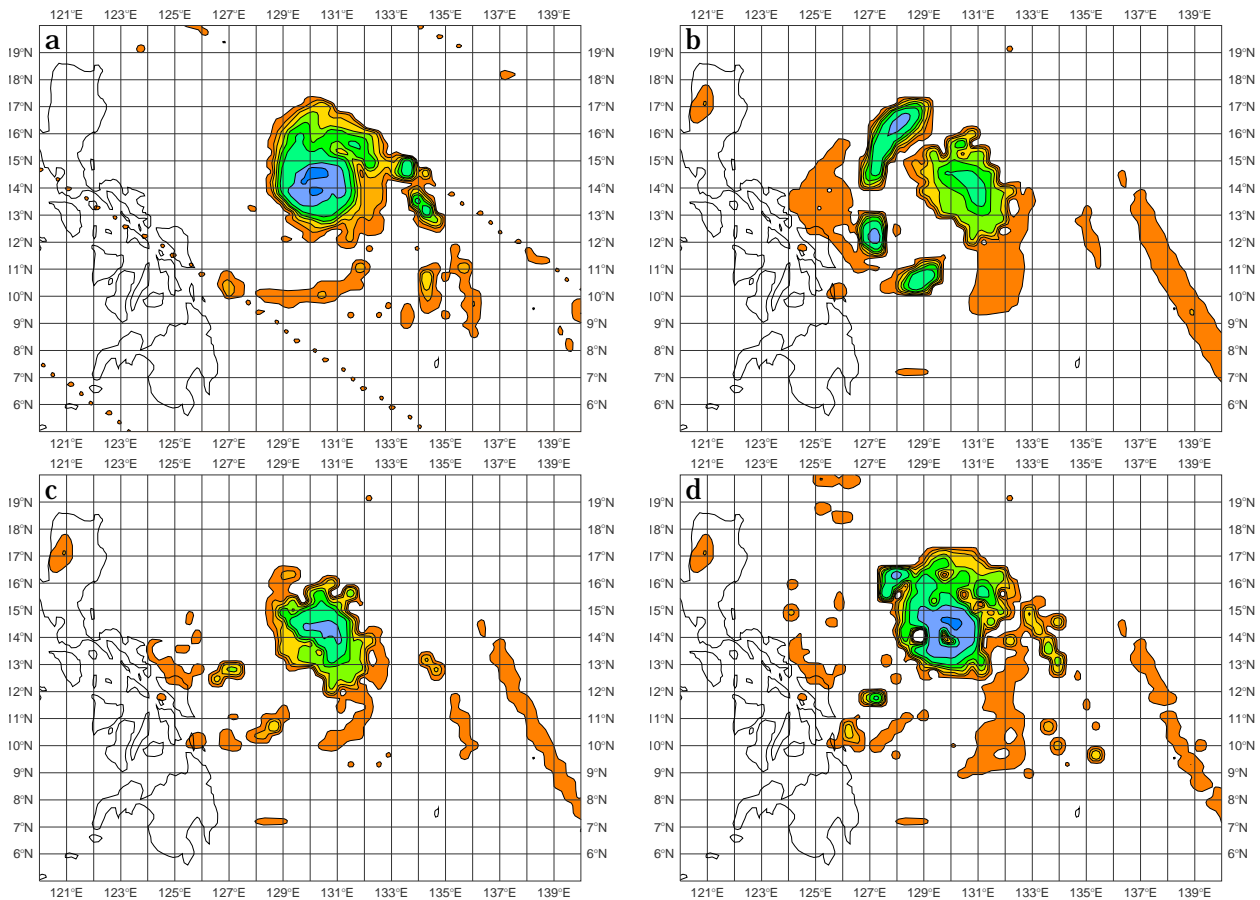
Figure 20: 1DVar assimilation of TRMM Microwave Imager (TMI) observations. (a) Observed rainfall rates as retrieved from TMI using the so-called 2A12 algorithm. (b) Model rainfall rates before assimilation, i.e. the background. (c) Model rainfall rates after assimilation with Method-1 using TMI 2A12 rainfall rates. (d) Model rainfall rates after assimilation with Method-3 using TMI microwave radiances (10H-V, 19H-V, 22V, and 37H-V GHz channels). Contour levels are 0.1, 0.5, 1, 2, 3, 5, 10, 20 mm h^{-1}.

in the operational code, which will ease adjoint developments. A new formulation is used for the entrainment rate. The triggering and initial characteristics of the convective updrafts that originate from the surface are now directly related to the surface turbulent heat fluxes, following some ideas by Siebesma and Jakob (2002). Simplified representations of the effects of downdrafts and convective momentum transport are also included.

The new convection scheme has first been validated in the single-column version of the ECMWF model and then in the full 3D model for periods of up to four months. In the context of such standard forecasts, the new parametrization has turned out to behave similarly to the more sophisticated operational scheme. The sensitivities of the outputs of the modified convection scheme to its input temperature and specific humidity variables have been studied for a set of several hundred initial atmospheric profiles, using the Jacobian method. This approach has permitted efficient identification and modification of portions of the code that could lead to excessive and thus undesirable sensitivities. After these modifications, the vertical profiles of the Jacobians of convection are smoother with the new parametrization than with the operational one, and the domain of validity of the linear assumption now extends to larger perturbations. This scheme was used for the assimilation experiments shown in Fig. 20.

5.4.2   Linearized cloud parametrization

Work on the assimilation of clouds has started recently in a 1D-Var framework where both observations from TOVS radiances (Chevallier *et al.* (2001b)) and broadband longwave fluxes from ARM field campaign (Janisková *et al.* (2002)) have been used. The numerical tools to compute cloudy and rainy radiances from various platforms (ATOVS, SSMI, Meteosat) have been developed and used to evaluate the ECMWF moist physics (Chevallier *et al.* (2001a); Chevallier and Kelly (2002)). It has been shown that the 1D-Var retrieval is capable of generating and removing clouds as necessary. A physical linearized cloud scheme is now the main missing element.

5.4.3   Required enhancements of the 4D-Var system

Regarding the assimilation system itself, an important requirement is a better consistency between the inner and outer loops of the 4D-Var in terms of resolution, variable representation and time integration scheme for humidity.

In the forthcoming revision of the 4D-Var solution-algorithm (due for implementation in the autumn 2002), the low-resolution linearization trajectory is created through interpolation of the high-resolution fields. This will ensure that model profiles are similar at inner and outer loops, and that physical processes (i.e. those associated with cloud and rain) are active at similar locations at both high and low resolution. The revision will also allow further increases in inner-loop resolution (to T_L255 and beyond), when appropriate, depending on the availability of accurate linear physics (at high resolution), and on the availability of high-resolution observations.

The inclusion of physical processes as observation operators will increase the non-linearity of the assimilation system and more outer loops may be necessary for an improved convergence of the minimization. In the forthcoming autumn-2002 revision, one additional update of the outer-loop is envisaged, i.e. an increase from two to three outer-loop updates.

For Method-4, a technical reorganization of the observation operators will be required, to make available to the RT-model the cloud parameters of the moist-physics parametrizations. So far physical parametrizations on the one hand and the observation operators on the other, have been considered as separate entities. However, for direct assimilation of cloudy and rainy radiances, it is envisaged that the RT calculations will need to be performed in immediate proximity of the model physics. Therefore its is planned to perform the RT-model calculations on the model's reduced Gaussian grid, for each satellite instrument in question, and then to interpolate the calculated radiances to the observation locations.

Finally, improvements to the formulation of the humidity analysis (the choice of control variable, the statistics of background errors) should also be very beneficial for the assimilation of clouds and precipitation. These developments are described in the following section.

6   A new formulation of the humidity analysis

At the present level of analysis accuracy, the background errors for all control variables except humidity appear to have near-normal distributions, which can be approximated by Gaussian pdfs. Gaussian pdfs are very convenient as they are fully determined by their variance alone (assuming zero mean). The use of Gaussian pdfs in a variational analysis furthermore results in a quadratic cost-function, which is more easily minimised than that of the general (non-Gaussian) case. Initial studies have shown that humidity has the least Gaussian and

the least homogeneous background errors of all the analysis variables. It is suspected that the non-Gaussian behaviour is a major contributor to problems in the humidity analysis, which have until now required *ad hoc* 'fixes'. Examples of such fixes and motivation for their existence can be found in Andersson *et al.* (1998), affecting the humidity impact of radiosonde geopotential data, in Simmons *et al.* (1999), affecting the stratospheric humidity analysis, and in Andersson *et al.* (2000), affecting the use of water-vapour-sensitive radiance observations. In the latter case it was shown that the background-error covariance model for humidity resulted in excessively large background errors in terms of the observed quantity (water-vapour radiances), especially in some sub-tropical regions, giving this type of data far too high weight in the analysis. The aim of the present re-formulation is to rectify some of these shortcomings of the current humidity analysis.

In order to progress substantially with the humidity analysis it was felt necessary to first improve the description of the humidity background errors to the same level of accuracy as for other variables, and then in a second step to improve also the characterization of humidity observation errors. This should facilitate the removal of most or all of the 'fixes' mentioned above.

Since the humidity errors are non-Gaussian and inhomogeneous, both of these aspects must be built into the humidity covariances. This means that flow-dependent covariance models are needed. Non-linear diffusion equations (Weaver and Courtier (2001)) or recursive filters (Purser *et al.* (2002)) can be used, but we can achieve similar results by changing the humidity control-variable to one in which the errors are more nearly Gaussian and homogeneous. By a Gaussian control variable we mean that the background error of the variable, sampled over all gridpoints globally, has a near-Gaussian distribution. The change-of-control-variable approach has the advantage of easy implementation into the present spectral or wavelet formulation (Fisher and Andersson (2001)) of the background term.

There are several challenges associated with the proposed approach. The ECMWF analysis consists of a series of minimizations (inner loops) linearized around a reference state, non-linearly updated at outer-loop level. For the inner loops a control variable that is linearly related to the model variables is required, but there is no such restriction in the outer loops. We seek a linearized change-of-variable operator for the inner loops, with ways to include the non-linearity in the outer loops. Humidity errors are also to some extent correlated with errors in other analysis variables, and this also needs to be taken into account in the background error covariance model. These correlations are mainly expressions of thermodynamic and dynamic relationships, which may need to be characterized accurately.

6.1 Study of humidity forecast differences

We do not have knowledge of the true background errors. However, we do have sets of forecast differences which can be used as proxies for background errors. The forecast differences have been generated by an ensemble of data assimilations, with randomly perturbed observations (Fisher and Andersson (2001)). Consider two forecasts of the truth x, x_1^b and x_2^b, where

$$x_i^b = x + b^b(x) + \varepsilon_i^b \tag{1}$$

with b^b the bias and ε^b the stochastic error. The difference between forecasts is

$$x_1^b - x_2^b = \varepsilon_1^b - \varepsilon_2^b \tag{2}$$

We know that ε_1^b and ε_2^b are independent stochastic variables with the same pdf $P^b(\varepsilon^b)$. Then for $\delta x = \varepsilon_1^b - \varepsilon_2^b$,

$$P_C^b(\varepsilon_1^b - \varepsilon_2^b) = P_C^b(\delta x) = \int_{-\infty}^{\infty} P^b(\varepsilon_1^b) P^b(-(\delta x - \varepsilon_1^b)) d\varepsilon_1^b \tag{3}$$

From this we see that the forecast error differences are a convolution of the background errors with themselves with a pdf $P_C^b(\varepsilon_1^b - \varepsilon_2^b)$. If $P_C^b(\delta x)$ is Gaussian with variance σ^2, it can be shown that $P^b(\varepsilon^b)$ is also a Gaussian and with variance $\sigma^2/2$. Therefore it is of particular interest to find a Gaussian description of the forecast differences, since this directly translates into a Gaussian description of the background errors.

To study the error distribution of different humidity variables we create histograms of the forecast differences. The forecast differences are between two forecasts valid at the same time, where each forecast comes from a different member of the ensemble of assimilations. Each assimilation uses the same set of observations with different random perturbations added to each observation (with variance given by the observation errors). Initially, it is enough to consider just one set of forecast differences (about 140000 gridpoints per level) to get a good idea about the statistical behaviour of the errors. Through studying various candidates for the control variable, two results have emerged:

- Forecast differences for q, $\log q$ and RH at a given model level (near 850 hPa) show exponential-like, rather than Gaussian, error distributions (Fig. 21, left). The same was found to be the case for several other humidity variables. For the particular level shown here, the q distribution deviates more from a Gaussian than $\log q$ and RH.

- The forecast differences for a limited geographical region and/or similar values of the background fields are easier to approximate with a Gaussian. For the same 850 hPa model level difference we plotted the distribution of differences in a 2.5% interval centered around the median of the background values of each variable (Fig. 21, right). Here q and $\log q$ still have an exponential distribution, whereas RH now appears more nearly Gaussian. The form of these distributions varies from level to level and for different values of the background. There are circumstances in which RH is definitely not Gaussian (close to $RH = 0$ and $RH = 1$), and where instead $\log q$ appears almost Gaussian (close to the surface).
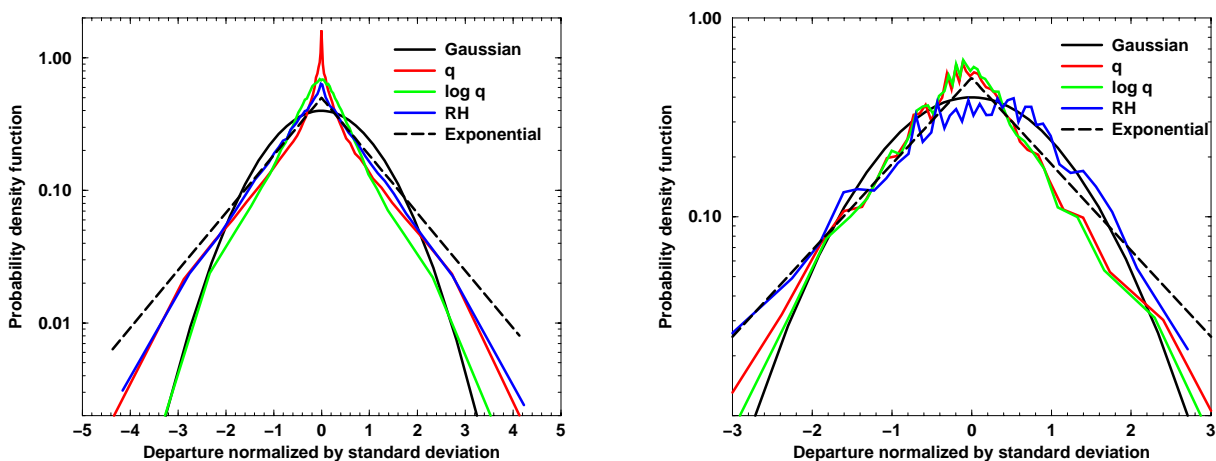

Figure 21: The pdf for a single forecast difference at approximately 850 hPa for q, $\log q$ and RH (see legend). The left panel shows all differences, and the right panel shows differences for similar values of the background field (a 2.5% interval centered around the median of the background values of each variable). For comparison, a Gaussian (black line) and an exponential pdf (dashed black) are also shown. The right panel is noisy due to the limited sample in each interval, but the result remains similar when more fields are added to the statistics.

6.2 Construction of a Gaussian control variable

The explanation for the results in the previous section is that the total distribution we see at each level is an integral over different conditions, each with its characteristic errors. The forecast difference $\delta\varphi$ of a given humidity variable $\varphi(q, T, p)$ can be studied as a function of the background, for example as a function of φ itself. The conditional error distribution $P(\delta\varphi|\varphi)$ varies with φ, and the total distribution is

$$P(\delta\varphi) = \int_{-\infty}^{\infty} P(\delta\varphi|\varphi)d\varphi \tag{4}$$

This function is generally not Gaussian. Even if $P(\delta\varphi|\varphi)$ were Gaussian for all values of φ (with standard deviation $\sigma(\varphi)$ and bias $b(\varphi)$), $P(\delta\varphi)$ would more probably be exponential due to the variation of σ and b with φ. A special case, which would give Gaussian $P(\delta\varphi)$ is if σ and b were constants. This motivated our approach for constructing a Gaussian control variable:

- Find a variable φ whose forecast difference $\delta\varphi$ follows a Gaussian conditional error distribution $P(\delta\varphi|\Phi)$ as a function of some variable Φ. This means that the background conditional error $P^b(\varepsilon^b|\Phi)$ will also be Gaussian, with variance $\sigma^2/2$. In practice a near-Gaussian distribution will be sufficient.

- Determine the bias and standard deviation of the forecast differences as a function of Φ. From a practical point of view, we would like the bias $b(\Phi)$ to be negligible. The reason is that if the minimum of the costfunction $J_b(\delta x)$ is not at $\delta x = 0$, then we will have non-zero analysis increments even if there are no observations.

- Normalize the forecast differences by the bias and standard deviation,

$$\widetilde{\delta\varphi} = \frac{\delta\varphi - b(\Phi)}{\sigma(\Phi)} \tag{5}$$

  Note that if we have managed to find $\widetilde{\delta\varphi}$ following this procedure, then the forecast differences will be uniformly Gaussian for all levels taken together, with zero bias and a standard deviation $\sigma_{\widetilde{\delta\varphi}} = 1$.

- In terms of the analysis formulation this implies a change to the control variable according to Eq.5, with Φ chosen such that the bias is negligible and with the forecast difference standard deviation $\sigma(\Phi)$ replaced by $\sigma(\Phi)/\sqrt{2}$.

6.3 Normalized relative humidity as control variable

After experimenting with several possible formulations of the control variable, it was found that relative humidity RH had reasonably homogeneous statistics. However, as shown in Fig.21 using δRH as a control variable is inappropriate as it has an exponential error distribution. Normalization $\widetilde{\delta RH} = \frac{\delta RH - b(RH^b)}{\sigma(RH^b)}$ gives near-Gaussian distributions for median values of RH^b, but the distribution tends to be asymmetric for extreme values of RH^b. This is expected since $P(\widetilde{\delta RH}|RH^b)$ is skewed towards negative values for large RH^b and positive values for small RH^b (see Fig. 22, left). An additional problem with this choice of control variable is a non-negligible bias (Fig. 22, right), which is not easily accounted for in the formulation of the analysis.

From the study of forecast differences we can see that there is a way to avoid bias and asymmetry. If we have two forecasts RH_a and RH_b, then $P(RH_a - RH_b|RH_a)$ and $P(RH_a - RH_b|RH_b)$ are antisymmetric. This is easily checked by plotting the corresponding graphs (not shown). This antisymmetry can be explained by rewriting
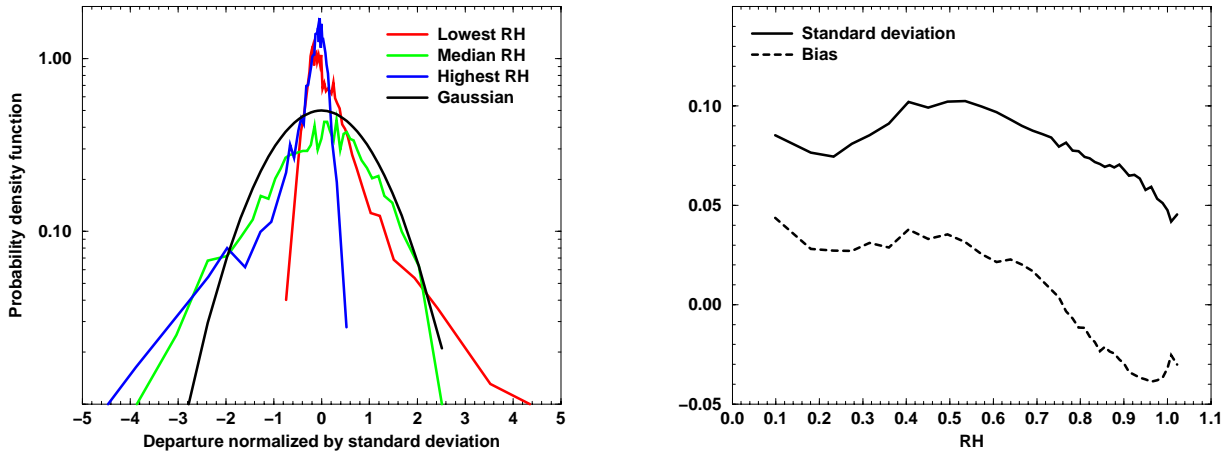
Figure 22: Forecast differences for the 'linear' $\delta RH(RH^b)$ at approximately 850 hPa. The left panel shows the pdf's for the lowest, median and highest 2.5% values of RH^b, and the right panel shows the standard deviation (full line) and bias (dashed) as a function of RH^b.

$P(RH_a - RH_b|RH_b)$ as $P(-(RH_b - RH_a)|RH_b)$ and noting that since RH_a and RH_b follow the same distribution, they can change place in the calculation of the statistics, so that $P(RH_a - RH_b|RH_b) = P(-(RH_a - RH_b)|RH_a)$. From this follows that if we stratify the statistics of $\delta RH = RH_a - RH_b$ according to the average of the forecasts we get the symmetric distribution $P(RH_a - RH_b|\frac{1}{2}(RH_a + RH_b)) = P(\delta RH|RH_b + \frac{1}{2}\delta RH)$. The result is shown in Fig. 23. The control variable is thus $\widetilde{\delta RH} = \frac{\delta RH}{\sigma(RH^b + \frac{1}{2}\delta RH)}$. The bias is effectively eliminated with this choice of control variable (Fig. 23, right).
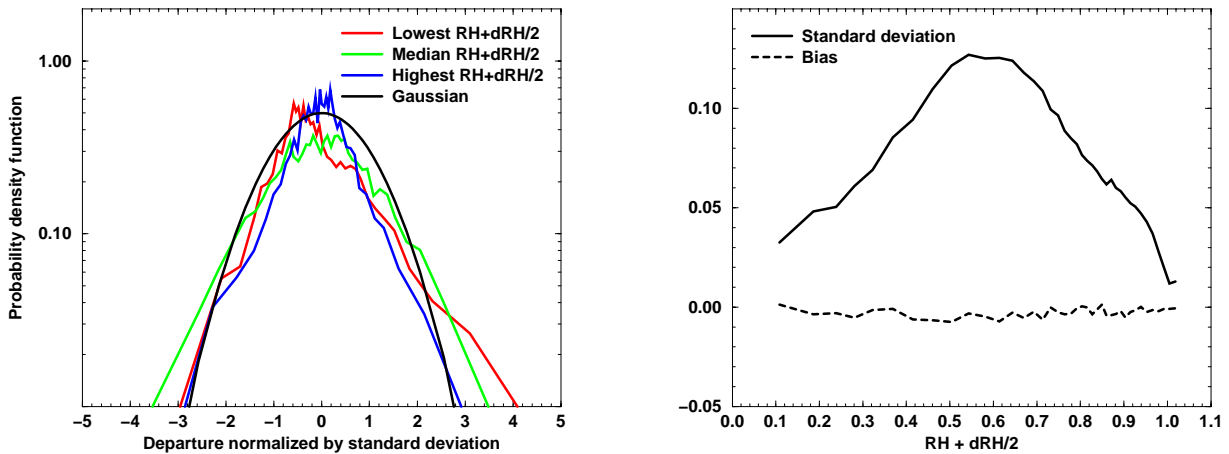

Figure 23: Forecast differences for the 'symmetric' $\delta RH(RH^b + \frac{1}{2}\delta RH)$ at 850 hPa. The left panel shows the pdf's for lowest, median and highest 2.5% values of $RH^b + \frac{1}{2}\delta RH$, and the right panel shows the standard deviation and bias as a function of $RH^b + \frac{1}{2}\delta RH$. All three curves compare reasonably well with the Gaussian (black line). Note that bins for the extreme values of RH^b are particularly affected by model and analysis effects of super-saturation clipping and resetting of humidity to positive values.

An alternative way to derive a Gaussian control variable would be to define a non-linear transformation $f(\delta\varphi, \Phi)$ directly, based on forecast error differences. As we have seen in previous sections, it is necessary to make the transformation a function of the background conditions to achieve near-Gaussian distributions for all conditions. The way to achieve this is to base the 'gaussianization' transform on the conditional pdf $P(\delta\varphi|\Phi)$ instead of basing it on $P(\delta\varphi)$. For a given Φ, we just need to find a transformation $f(\delta\varphi, \Phi)$ of the $\delta\varphi$ axis such that the probability that $x \leq \delta\varphi$ equals the probability that $\xi \leq f(\delta\varphi, \Phi)$ for a normal Gaussian distribution,

$$\Pi(\delta\varphi|\Phi) = \int_{-\infty}^{\delta\varphi} P(x|\Phi)dx = \int_{-\infty}^{f(\delta\varphi,\Phi)} \frac{1}{\sqrt{2\pi}} e^{-\xi^2/2} d\xi = \Pi_G(f(\delta\varphi, \Phi)) \tag{6}$$

where Π are the cumulative pdf's. Inverting the Gaussian cumulative distribution then gives

$$f(\delta\varphi, \Phi) = \Pi_G^{-1}(\Pi(\delta\varphi|\Phi)) \tag{7}$$

This will always work, but may result in a bias term, which does not easily fit into the analysis framework, as has been explained above. However, we could apply this transform as a finishing step after the symmetrizing transform and in that way avoid the bias term. This approach makes the search for a Gaussian control variable automatic, although it does not guarantee the best control variable. There may be another choice, which is less non-linear for example.

For the normalized relative humidity control variable, we do not need to apply this final 'gaussianization', since the departures are already close to Gaussian. But if there is no other way to find a reasonably Gaussian control variable, this approach can always be applied.

6.4 Implementation of the humidity control variable, using a linear change-of-variable transform

The difficulty with the symmetric control variable is that a non-linear variable transform is needed to go from the model to the control variable. This non-linearity is unavoidable when converting from non-Gaussian to Gaussian control variables. We can use the non-linear symmetrizing transform when going between inner and outer loops of the analysis, and use a linearization around the latest outer loop in the inner loops. We will now first describe a linear implementation, which has been used in the experiments with the new humidity control variable reported below. The linear implementation covers most of the developments needed for a non-linear implementation, including the calculations of the covariance matrices which will be the same in both the linear and the non-linear implementation.

6.4.1 The linear humidity control variable

The change of variable from specific humidity to normalized relative humidity has two steps. First relative humidity increments are calculated from temperature, pressure, and specific humidity increments. Then the relative humidity increment is normalized by the standard deviation which applies for the particular relative humidity value.

For the first step, we replace the non-linear relation for relative humidity,

$$RH(p, q, T) = \frac{pq}{\varepsilon e_s(T)} \tag{8}$$

by a linear relation for the relative humidity increments. Denote the non-linear reference state $\vec{x}$ so that $\vec{x} = \vec{x}^b + \delta\vec{x}$. The reference state is the background in the first outer loop, and the updated non-linear trajectory in

subsequent outer loops. Since the saturation vapour pressure $e_s(T) = a_1 e^{a_3(T-T_3)/(T-a_4)}$ is exponential in T, we linearize the logarithm of relative humidity, which gives

$$\delta RH \approx RH^b \left(\frac{\delta p}{p^b} + \frac{\delta q}{q^b} - \frac{\delta T}{\alpha_T^b} \right) \tag{9}$$

Here $\alpha_T^b = (T^b - a_4)^2 / [a_3(T_3 - a_4)]$. This linearization is quite accurate for all ranges of values, which has been verified by a scatterplot between non-linear and linearized forecast differences (not shown).

For the second step, we need to divide by $\sigma(RH^b + \frac{1}{2}\delta RH)$, but this is again a non-linear operation, so we replace it by

$$\widetilde{\delta RH} \approx \frac{\delta RH}{\sigma(RH^b)} \tag{10}$$

This approximation should converge to the right solution, since δRH becomes smaller in each subsequent outer loop through the updating of the reference state. Exceptions are possible at low relative humidity, where positive humidity increments can become too small, and close to saturation for negative increments. On the other hand, tendencies for supersaturation and negative humidity are correctly suppressed (although not necessarily avoided). So this first linear implementation is expected to be robust, while erring on the side of caution and ignoring some observational information in very dry and saturated conditions.

Expressed in matrix form, the linear change of variable is

$$\begin{pmatrix} \delta T \\ \delta p \\ \widetilde{\delta RH} \end{pmatrix} = \begin{pmatrix} 1 & 0 & 0 \\ 0 & 1 & 0 \\ -\frac{RH^b}{\sigma(RH^b)} \frac{1}{\alpha_T^b} & \frac{RH^b}{\sigma(RH^b)} \frac{1}{p^b} & \frac{RH^b}{\sigma(RH^b)} \frac{1}{q^b} \end{pmatrix} \begin{pmatrix} \delta T \\ \delta p \\ \delta q \end{pmatrix} \tag{11}$$

The normalizing standard deviations are estimated from the gridpoint differences of forecasts from an ensemble of 4D-Var analyses with perturbed observations. Only a few tens of differences are needed since even one set of forecast differences gives the general behavior, with subsequent forecast differences mainly reducing the noise in the statistics. At each level, the behaviour of the standard deviation of δRH as a function of $\xi = RH^b + \frac{1}{2}\delta RH$ is replaced by a piecewise polynomial $P_k(\xi)$ at each level k, with $P_k(0) = 0$ and $P_k(\xi)$ increasing linearly for $\xi > 1$, all according to the forecast difference statistics. This makes the relative humidity background error a function of relative humidity and pressure, whereas the present operational formulation is a function of relative humidity and temperature (Rabier *et al.* (1998)).

In the experiments with the linear control variable the humidity analysis was cleaned up by removing all 'fixes' to do with particular shortcomings of the current specific-humidity formulation (as mentioned above). These fixes included controls of negative and supersaturated humidity and suppression of humidity increments in the stratosphere. With the re-formulated humidity analysis these fixes should no longer be required. The re-formulation is achieved by supplying new covariance matrices (for the normalized humidity variable), and new routines to perform the change of variable transformations. This also makes the humidity analysis formally more similar to the analysis of the dynamic variables.

A major difference with the new control variable is that in principle it is analyzing relative rather than absolute changes in humidity. Correlations between the stratosphere and the troposphere are therefore not as dangerous as before, when a small tropospheric increment could lead to a relatively large stratospheric increment due to the differences in absolute humidity values. However, an increment from a humidity observation located in a very dry area could now have its maximum located away from the observation if there is a large gradient in the absolute humidity. To address this potential problem, the correlations need to be even more flow dependent with a built in dependence on the gradients in the background fields.
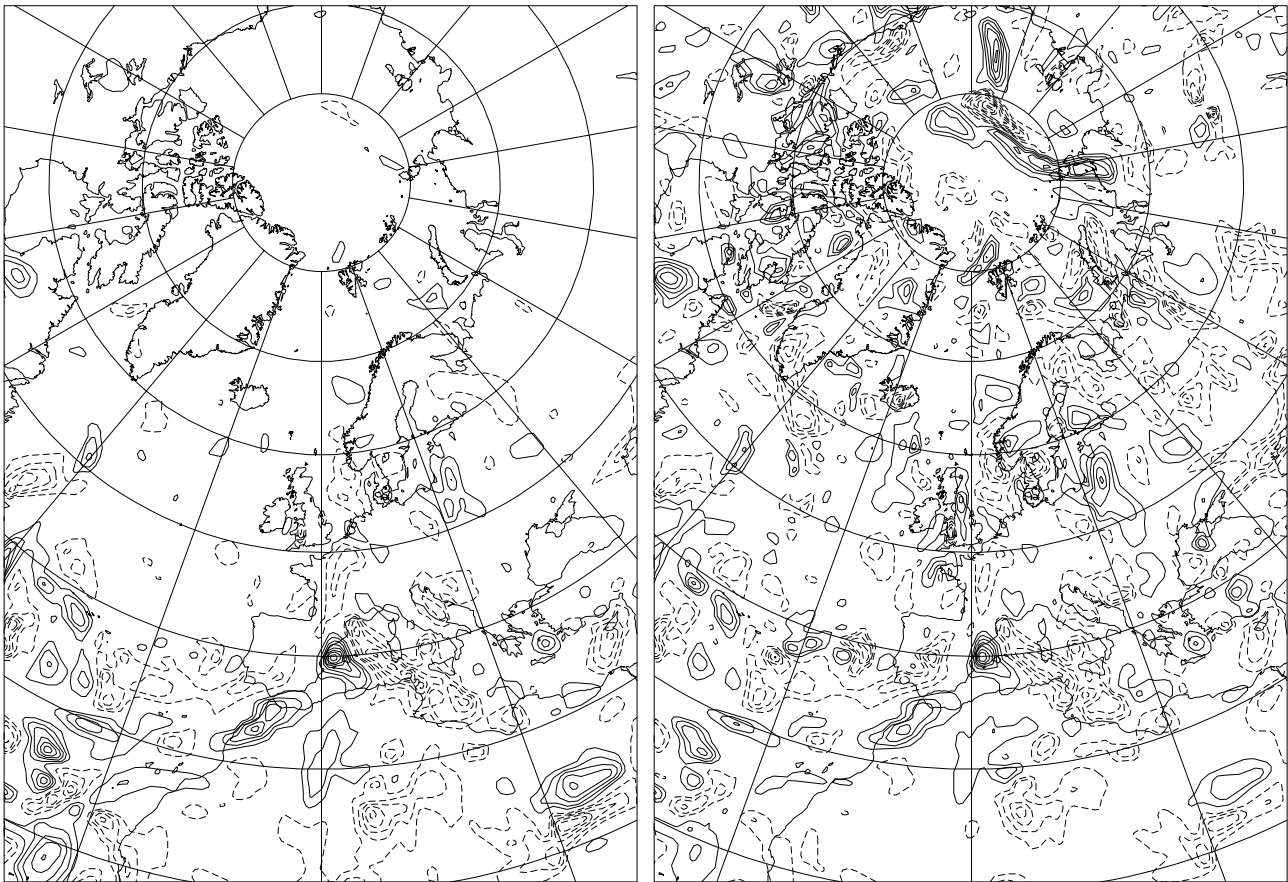
Figure 24: Forecast differences for specific humidity δq (left, isolines 0.005 g/kg) and normalized relative humidity $\widetilde{\delta RH}$ (right, isolines 1) at a single level (approximately 850 hPa). The two fields show what are the inputs to the statistical determination of covariance matrices for the two variables. Normalized relative humidity is more homogeneous.

The linear normalized relative humidity control variable has some similarities with the pseudo-relative humidity q/q_s^b introduced by Dee and Da Silva (2002). The additional features in the present approach are the normalization to achieve more gaussian statistics and the multivariate relation with temperature and pressure.

6.4.2 *Background-error covariances*

The background-error covariance matrices for the new normalized relative-humidity control-variable are calculated from around 120 pairs of spectral forecast differences from the 4D-Var ensemble of analyses in exactly the same way as for the other variables. The advantage of calculating the covariance matrices in terms of normalized relative humidity instead of specific humidity is seen in Fig. 24 where we show a comparison of the forecast differences of δq and $\widetilde{\delta RH}$ at approximately 850 hPa. These are the actual inputs for the calculation of the covariances. The transformed relative humidity shows a homogeneous difference field, which is much easier to characterize statistically than the inhomogeneous specific humidity difference field. Compared with specific-humidity covariances calculated from the same set of forecast differences, the correlations are now sharper in the vertical (Fig. 25). However, the stratospheric part should be treated with caution in both cases since stratospheric humidity increments were suppressed in the currently available assimilation ensemble. The horizontal correlation length scales are also smaller in the stratosphere with the new formulation (Fig.26). The average spectral variances are now by construction nearly constant in the vertical, compared with nearly five

orders of magnitude variation in the vertical when specific humidity is used, Fig.27(left). This improves the condition number of the covariance matrix dramatically, from 10^6 to 10^2, see Fig. 27 (right). A normalized version of specific humidity would of course also give better conditioned covariances. This improvement should make it possible to perform the humidity analysis also in the stratosphere.
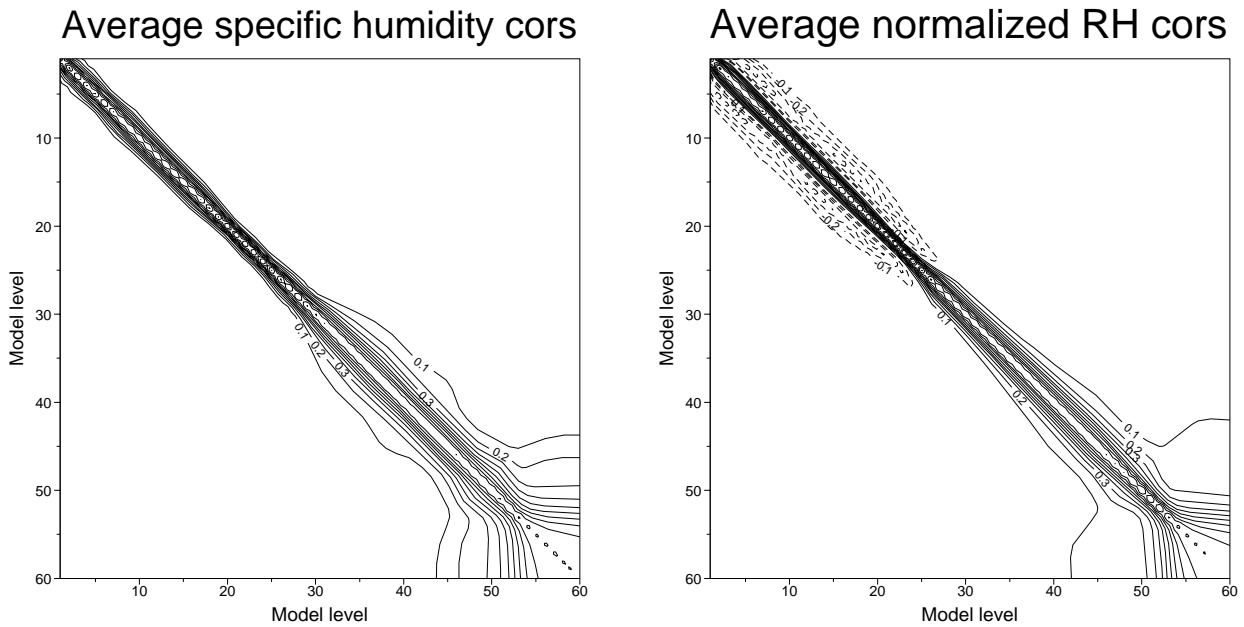

Figure 25: Average vertical correlations for specific humidity (left) and normalized relative humidity (right), for the 60 model levels.
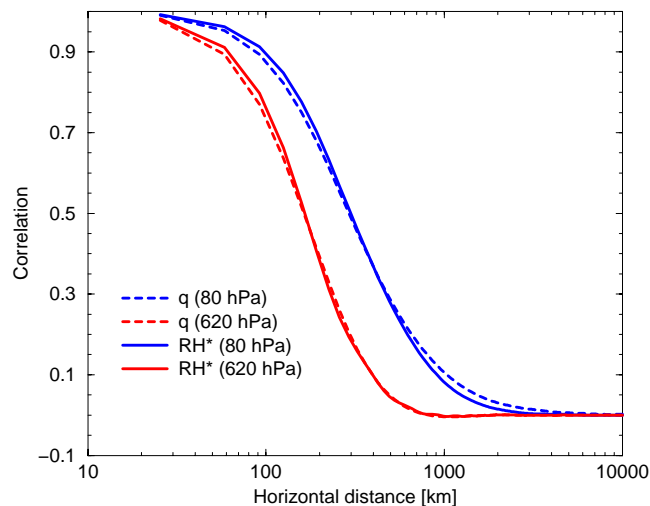
Figure 26: Average horizontal correlations for specific humidity and normalized relative humidity. A lower-stratospheric and a tropospheric level are shown.
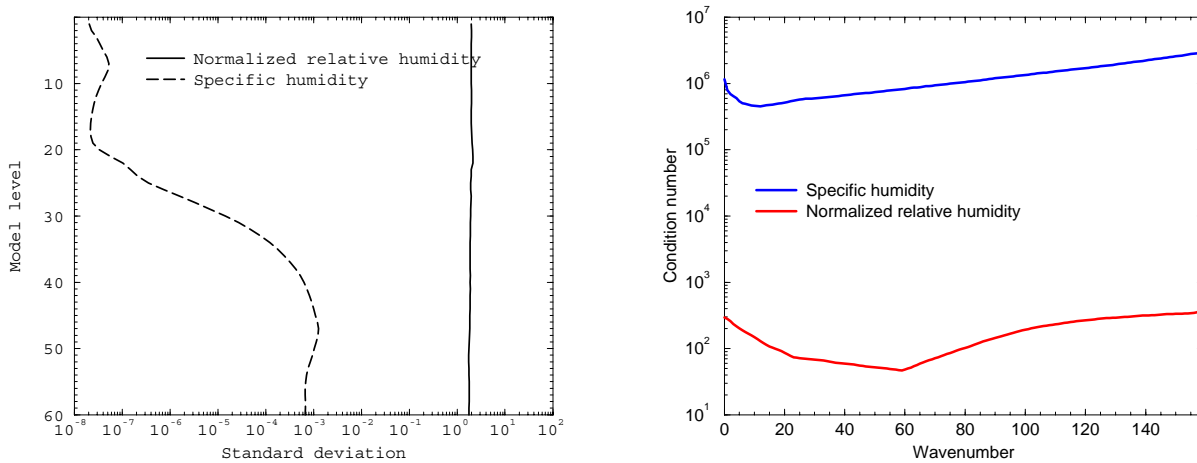
Figure 27: Average standard deviation at different levels (left) and condition numbers for different wavenumbers (right) for specific humidity and normalized relative humidity.

6.4.3 Stratospheric humidity analysis

It should now in principle be possible to perform a stratospheric humidity analysis, as the main problems related to the large variation of specific humidity with height have been solved. However, the timescale of humidity changes is very long in the stratosphere and at least one to two years of assimilation, including stratospheric humidity data, in an ERA-40 framework would be necessary to assess the stratospheric component of the analysis. Both the MLS and SAGE II stratospheric limb water-vapour profiles with a couple of kilometers vertical resolution are available for this purpose. A long assimilation experiment of this kind will help assess the effects of the changed humidity analysis on the whole hydrological cycle. We would also expect to recalibrate the errors of humidity-sensitive observations before performing a long assimilation of this kind. Also retrievals from the limb-sounding MIPAS instrument (soon to be available) on ENVISAT will be useful for validation of the stratospheric humidity analysis.

6.4.4 Single-observation experiments

To illustrate the behaviour of the linear implementation of the normalized relative-humidity control-variable we have performed a single-observation experiment. A single 500 hPa q observation is inserted in a North Atlantic frontal zone (50^oN 18^oW), where there is a strong gradient in humidity between a dry and a saturated region. For comparison, we show the same experiment performed with the present operational analysis formulation, which has specific humidity as control variable. The observation is located at the start of a 6-hour 4D-Var window, which is equivalent to performing a 3D-Var analysis in this case.

In Figs. 28 – 29 we see east-west cross sections through the specific humidity increments (at the observation latitude) for the operational and the new humidity control variable, respectively. The differences are largest in the saturated regions of the front. In the new formulation there are no supersaturation controls, but through the background dependency of the errors, the analysis recognizes the saturated regions and reduces the size of the increments accordingly to reduce supersaturation. In the operational formulation, the raw analysis increment is almost symmetric and decreases smoothly from a maximum at the observation location. In the present case, this leads to supersaturation. However, the operational formulation has a supersaturation check, which changes

the humidity after the analysis. This way of suppressing the supersaturation causes rough analysis increments.

In Fig. 30 we show the temperature and wind increments caused by the multivariate aspects of the new humidity control variable. The temperature increment is caused directly by the relative humidity change, and the wind increment comes from the dynamic temperature-wind correlation. This multivariate aspect is new compared to the operational formulation. The increments are quite small since the humidity observation is very close to the value of the background, but the structure of the increment would be similar for larger increments.
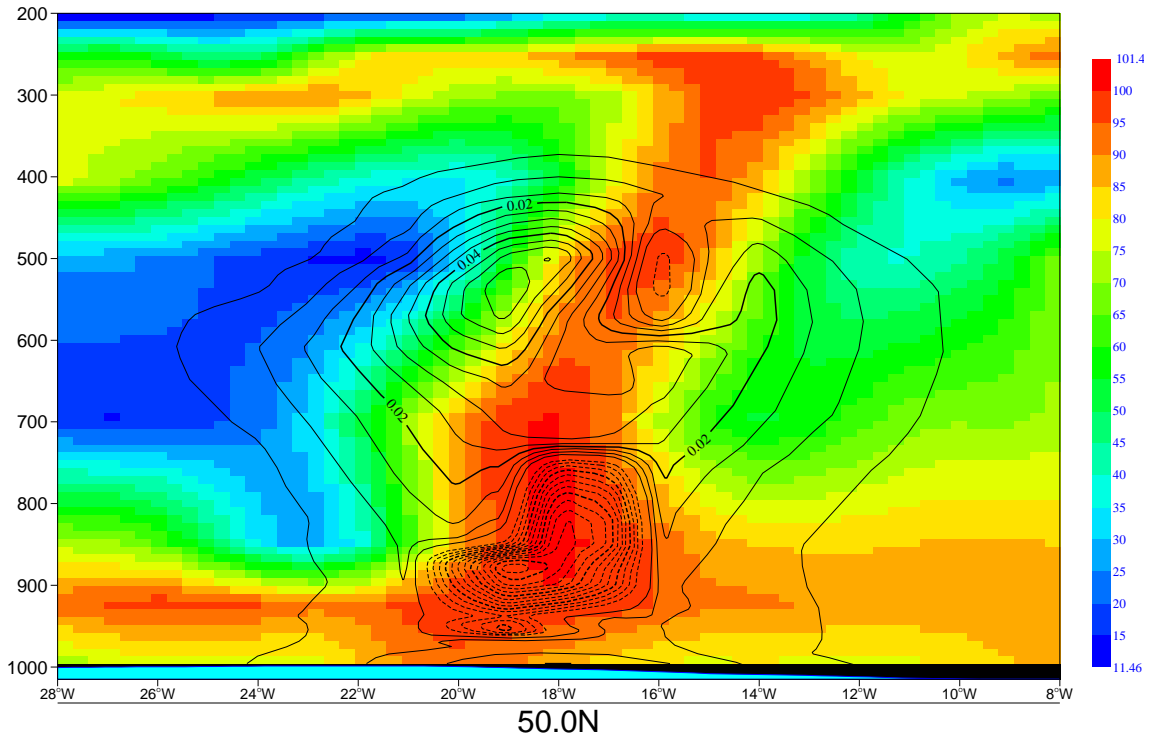
Figure 28: Specific humidity increment from a single q observation (500 hPa, $50\,^oN\,18^oW$) using the present operational δq control variable with associated supersaturation checks (isolines 0.005 g/kg). The shading shows the analyzed relative humidity (%).

6.5 Possible further developments of the humidity analysis formulation

6.5.1 A non-linear humidity control variable

An implementation of the non-linear humidity control variable described above involves an additional, modified updating of the trajectory at outer loop level. Each series of inner loops results in a new $\widetilde{\delta RH}$, which can be transformed back to δRH, and as we know the temperature and pressure increments, the specific humidity increment can be computed. Here we have no restriction that the transform should be linear, and the symmetric transform can be used. A possible implementation is as follows:

- At the begin of each analysis we know RH^b and $P(\delta RH|RH^b)$ (see Fig. 22 left). We need $\sigma(RH^b + \frac{1}{2}\delta RH)$, but δRH is unknown. However, from $P(\delta RH|RH^b)$ we can get the expected $<\delta RH>$ for the particular RH^b, which is just the bias in Fig. 22 right. In the first series of inner loops, use $\sigma(RH^b + \frac{1}{2} < \delta RH >)$ in the linearized change of variable.
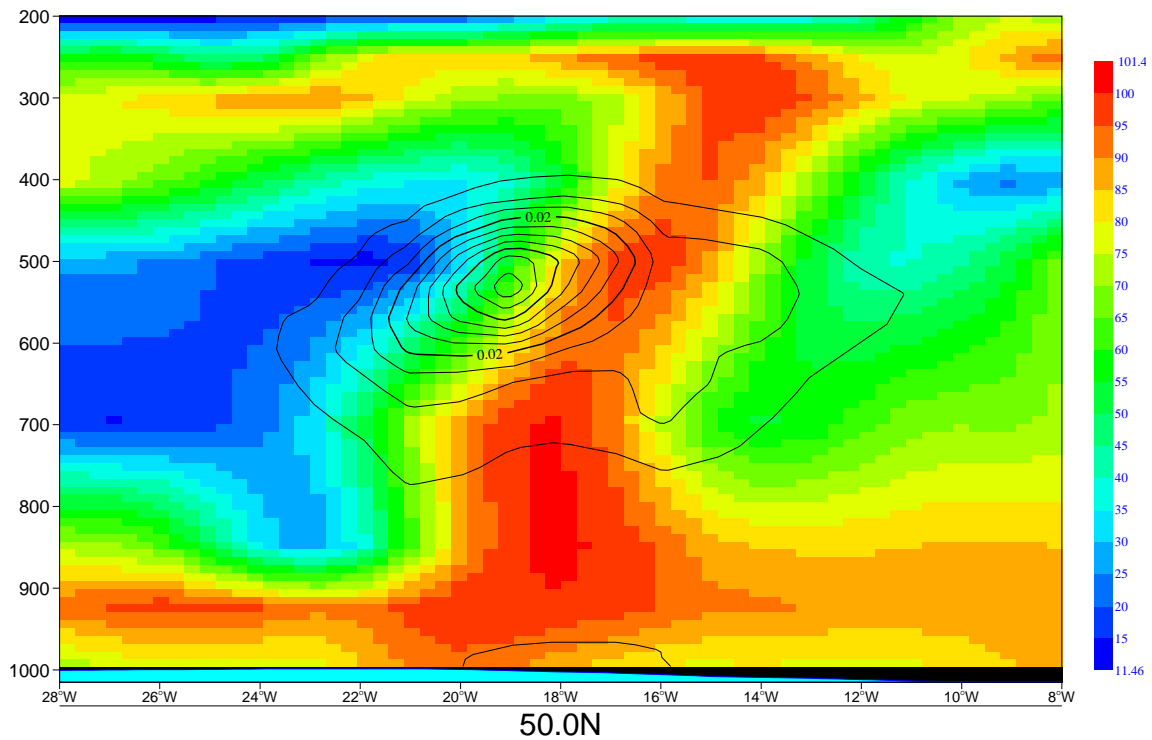
Figure 29: Specific humidity increment from a single q observation (500 hPa, $50\,^oN\ 18^oW$) using the $\widetilde{\delta RH}$ control variable (isolines 0.005 g/kg). The shading shows the analyzed relative humidity (%).
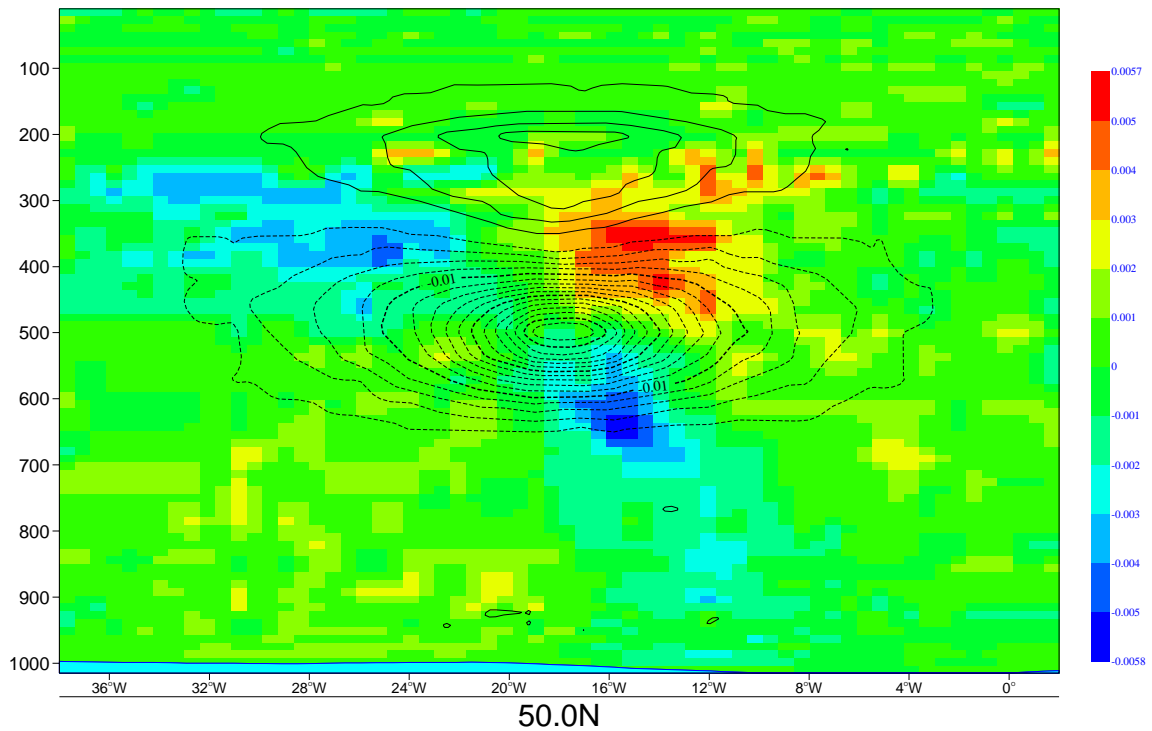

Figure 30: Temperature and u-wind increments from a single q observation (500 hPa, $50\,^oN\ 18^oW$) using the $\widetilde{\delta RH}$ control variable (isolines 0.002 K). The shading shows the wind increment (m/s).

- At the end of the first minimization we have $\delta RH^{(1)} = \widetilde{\widetilde{\delta RH}}^{(1)}\sigma(RH^b + \frac{1}{2} < \delta RH >)$. Undo the linear transform to get $\widetilde{\delta RH}^{(1)}$ and solve instead the symmetric transform $\widetilde{\delta RH}^{(1)} = \delta RH/\sigma(RH^b + \frac{1}{2}\delta RH)$. From the behaviour of $\sigma(RH^b + \frac{1}{2}\delta RH)$ the approximation $\sigma(RH^b + \frac{1}{2}\delta RH) \approx \sigma(RH^b) + \frac{1}{2}\delta RH\sigma'(RH^b)$ seems reasonable. This gives

$$\delta RH^{(1)} = \frac{\sigma(RH^b)\widetilde{\delta RH}^{(1)}}{1 - \frac{1}{2}\sigma'(RH^b)\widetilde{\delta RH}^{(1)}} \tag{12}$$

- In outer loop i, replace RH^b by $RH^b + \delta RH^{(i-1)}$ and repeat the above procedure.

With this (or a similar) approach it is possible to account for the asymmetric behaviour of the humidity background errors at low and high relative humidities.

6.5.2 *Correlation relations for humidity background-errors*

Background errors in humidity and other variables are related through errors in transport and thermodynamic processes. At present the humidity is analysed univariately at ECMWF (Courtier *et al.* (1998)), thus ignoring all correlations that exist between the humidity and the other fields. The fact that there is an incomplete understanding at present of these humidity correlations has motivated the univariate approach. Furthermore, even properly formulated correlations can degrade a multivariate analysis if there are serious weaknesses in the humidity background-error formulation.

The approach applied to correlation modelling at ECMWF (Derber and Bouttier (1999)) is to redefine the control variable for say humidity as what remains when the correlations with mass and wind errors have been removed. The remainder, which would in our case be called uncorrelated humidity, has errors orthogonal to all other control variables. For humidity, this approach has been investigated by Berre (2000). Work to include coupling between humidity and vertical motion is underway at several NWP centres and universities, using different approaches involving Richardson's equation, potential vorticity, the omega-equation, or the non-linear balance equation.

The de-correlation of the humidity control variable from the dynamic variables is one step towards a more accurate background error model. There are additional constraints on for example relative humidity, which the humidity increments need to satisfy. Without proper relative humidity constraints humidity can be added at levels where it may cause excessive saturation, which immediately rains out. We have here an example of how precipitation can act as a fast restoring mechanism in the hydrological cycle. Proper humidity constraints are thus essential for the propagation of observational information through the hydrological cycle. We can also see from this simple example that what is really needed is a covariance model incorporating not only humidity, but also liquid water, ice and precipitation. Moisture fluxes from the surface and soil moisture, which responds on a longer timescale, may also have to be incorporated.

6.5.3 *Towards the definition of an uncorrelated humidity control-variable*

As a first step towards multivariate humidity correlation modelling, we seek to redefine the humidity control variable such that its background errors are uncorrelated with temperature and pressure. The normalized relative humidity can be separated into a 'thermodynamically correlated' part with background errors proportional to temperature and pressure errors and an 'uncorrelated' remainder, which will be the new control variable. The

correlated part will actually include an element of dynamic correlations as well through the regression against total temperature errors.

The de-composition of the normalized relative humidity errors is shown in Fig.31 (left). We see that the main contribution comes from specific humidity errors, with temperature errors contributing significantly only at very high relative humidity. The pressure error contributions are negligible (see also Lorenc *et al.* (2000)). Close to saturation, the specific humidity and the temperature errors are positively correlated, with a weaker anticorrelation below 80% relative humidity (Fig. 31, right). The strong positive correlation close to saturation means that humidity and temperature changes go together in such a way that relative humidity is decreased. This correlation is probably a part of a more extensive thermodynamic relationship, which includes condensation and precipitation, but even applied to humidity and temperature on their own, this relationship can probably solve most of the problems related to excessive humidity. Here we see the value of stratifying the humidity error statistics according to relative humidity. Lumping the statistics together, we would not see the strong correlation at saturation.
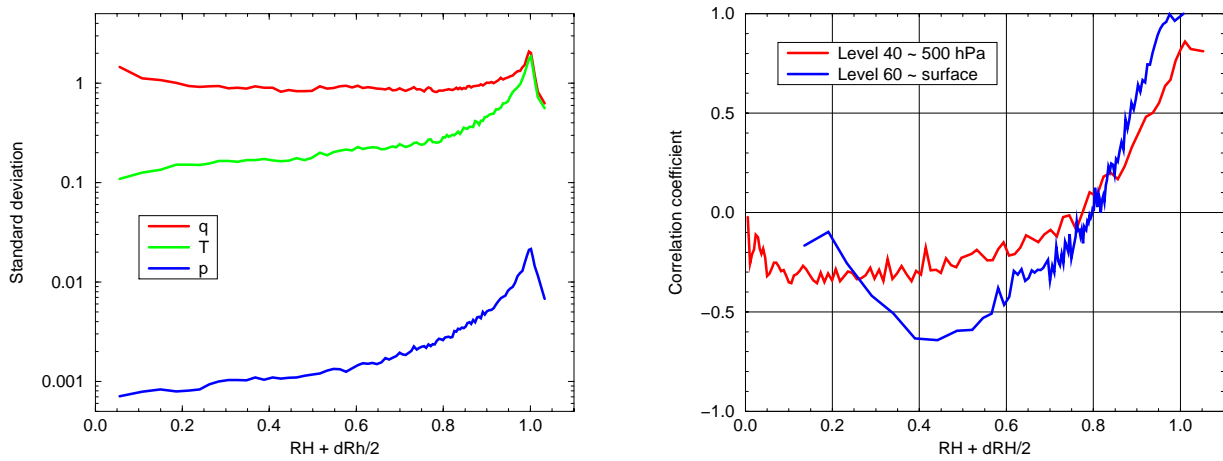

Figure 31: Left: Contribution of specific humidity (red), temperature (green) and pressure errors (blue) to normalized relative humidity errors at approximately 850 hPa. Right: Correlation between specific humidity and temperature contributions at approximately 500 hPa (red) and at the surface (blue). In both cases the statistics are plotted against $RH^b + \frac{1}{2}\delta RH$.

The uncorrelated humidity control variable could be implemented as follows. We know that the normalized humidity and temperature errors are related through a function of relative humidity,

$$\frac{\delta q}{q^b} = (\frac{\delta q}{q^b})_{unbal} + Q_k(\xi)\frac{\delta T}{\alpha_T^b} \tag{13}$$

where $\xi = RH^b + \frac{1}{2}\delta RH$ and $Q_k(\xi)$ is a polynomial approximation of the humidity–temperature regression (different at each model level k). As for the total relative humidity, we can normalize the uncorrelated humidity variable to get uniform error variances as a function of relative humidity,

$$\frac{1}{\sigma_q(\xi)}(\frac{\delta q}{q^b})_{unbal} = \frac{1}{\sigma_q(\xi)}\frac{\delta q}{q^b} - \frac{Q_k(\xi)}{\sigma_q(\xi)}\frac{\delta T}{\alpha_T^b} \tag{14}$$

or, simpler $\widetilde{\delta q}_u = \widetilde{\delta q} - Q_k(\xi)\widetilde{\delta T}$. In Fig. 32 we show the fraction of the variance in $\widetilde{\delta q}$ explained by the correlation with temperature as a function of relative humidity. The result is consistent with the behaviour seen previously in Fig. 31.
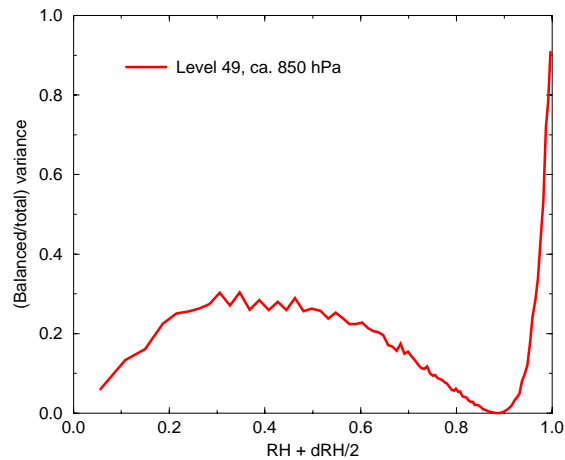
Figure 32: Fraction of $\widetilde{\delta q}$ variance explained by temperature at approximately 850 hPa (model level 49). We recall from Fig. 31 that above roughly 80% relative humidity, the humidity and temperature errors are positively correlated, but below 80% there is anticorrelation between the errors. The statistics are plotted against $RH^{b} + \frac{1}{2}\delta RH$.

6.5.4 *Illustrations of the multivariate aspects of the re-formulated humidity analysis*

As a simple illustration we investigate the response of the analysis to a perfect temperature observation for the different choices of control variables discussed above. Using specific humidity as control variable can lead to excessive supersaturation. Starting from a background relative humidity of 99% the specific humidity analysis gives 111% relative humidity (Fig. 33, left). The relative humidity based analysis is very close to the more accurate multivariate analysis. For an accurate description of the humidity background errors it is necessary to take into account the correlations between humidity and temperature. In terms of temperature observation response, a relative humidity based control variable is more accurate at high relative humidity, while a specific humidity based variable is more accurate away from saturation (Fig. 33, right). If we take the nonlinear version of the uncorrelated specific humidity as being the most accurate control variable, it can be seen that noticeable changes in behaviour could be expected when including both the correlations with other variables and the nonlinear behaviour in the humidity background error model. The control variable can be either relative or specific humidity based in this case, but the specific humidity version is simpler. A similar exercise could be done for a perfect humidity observation, but the present example suffices to show that it is worthwhile to develop the multivariate nonlinear version of the humidity analysis.

6.6 Trial assimilations of METEOSAT and SSMI radiance data, using the new humidity analysis formulation

The current operational humidity analysis gives excessively high weights to the 6-micron humidity-sensitive radiance data (METEOSAT water-vapour channel, and HIRS channel 12), in certain circumstances — mainly in dry subtropical air. This problem was investigated in detail by Andersson *et al.* (2000). It was found that the background error (σ_{b}), when expressed in terms of the observed quantity (i.e. brightness temperature for the radiance channel in question), showed very marked variations over the globe: from less than 2 K in many moist or cold regions, to 5-15 K in dry subtropical air. An example is shown in Fig. 34, where yellow shading starts at 7.5 K and orange at 10 K. The large ratio, locally, between between σ_{b} and σ_{o} (the observation error, set
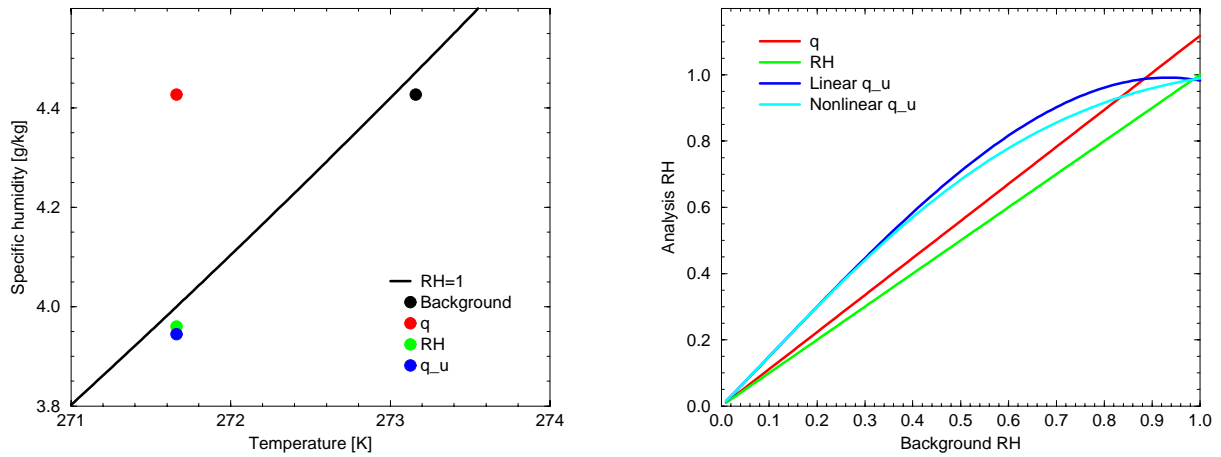
Figure 33: Analysis response to a perfect temperature observation for a background close to saturation (left) and as a function of relative humidity with fixed background temperature (right).
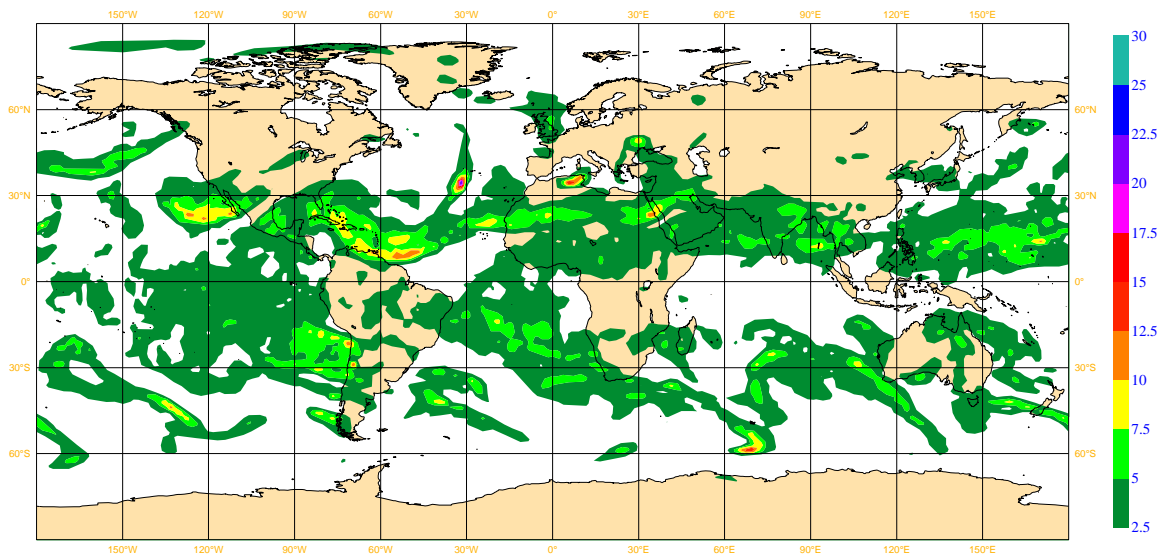

Figure 34: Background error standard deviations in terms of brightness temperature (K) for HIRS channel 12 (similar to the METEOSAT water-vapour channel), 20020124-18 UTC, computed using the method of Andersson *et al.* (2000), for the operational humidity analysis formulation. Shading starts at 2.5 K with an interval of 2.5 K
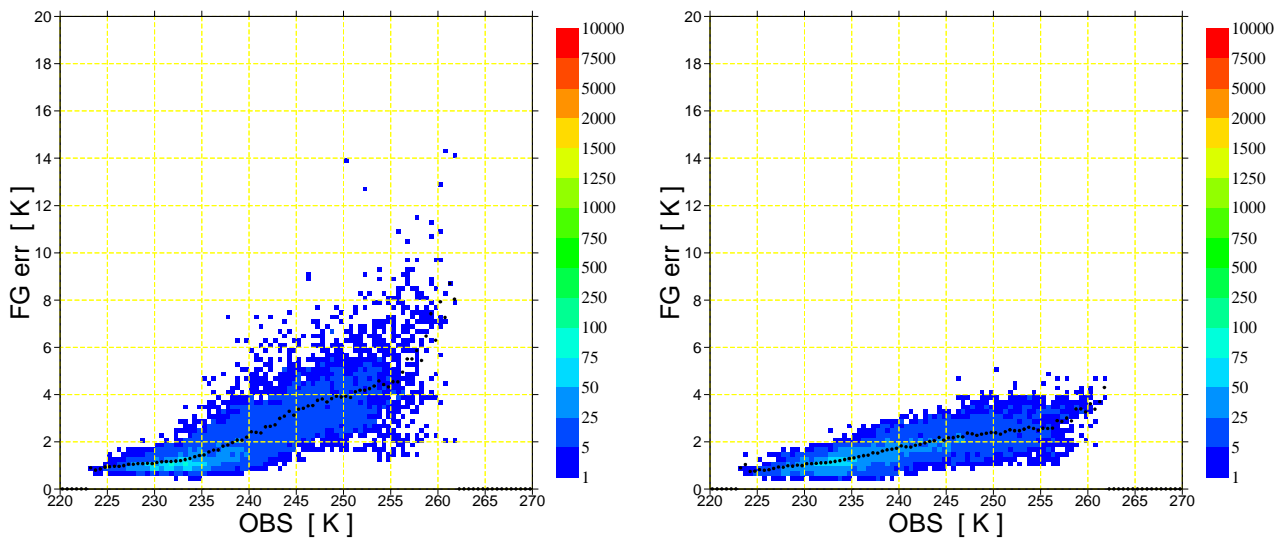
Figure 35: METEOSAT background-error standard deviation (K) as in Fig. 34, plotted against the observed brightness temperature value in the water-vapour channel, for the current (left) and the re-formulated (right) humidity analysis. The scatter density is coloured, see legend. The black curve indicates the median.

to 2.0 K) results in poor conditioning of the minimisation problem, and a slow rate of convergence. The large σ_b values are in contradiction with statistics of obsevation-minus-background departures — which have an rms of 2.5-5 K in dry sub-tropical regions. The corresponding map for the re-formulated humidity analysis is not shown here, but we can see from the scatter diagram in Fig. 35 that the values are less than 5 K everywhere (right panel) whereas they are in the range from 5 to 15 K with the current humidity analysis (left panel). In dry subtropical air (high observed brightness temperature) the median value of σ_b (the black line) is close to 4.5 K in the current humidity analysis. With the re-formulation it is close to 2.5 K, which is in good agreement with departure statistics, thus indicating that these data will get approximately the correct weight in the new humidity analysis.

The specific-humidity analysis increments are generally smaller in the re-formulated humidity analysis, as expected from the reduced background errors. Two examples are shown in Fig. 36 from a 3D-Var analyses using METEOSAT radiance data, only. The two vertical profiles of humidity increments are for the operational (blue) and the re-formulated (magenta) humidity analysis, respectively. The figures also show that there is less extrapolation of METEOSAT humidity increments to the lower troposphere, in the new humidity analysis.

In analyses using SSMI radiances only, the main difference due to the re-formulation is in the vertical extent of the increments, see Fig. 37. The size of the increments has been reduced (as for METEOSAT data), particularly at levels above model level 40, i.e. above 500 hPa (lower panel). The SSMI radiances have little information on the vertical distribution of humidity. We can see from the figures that the increments in both analysis (top two panels) are located primarily in the lower troposphere, above the boundary-layer (i.e. between 850 and 500 hPa, or model levels 50 to 39).

The analysis of total-column water-vapour is likely to change primarily in areas close to saturation. Fig.38 shows the difference in background error standard deviations in terms of TCWV (kg/m^2), between the re-formulated and the operational humidity formulation. The difference is generally negative, indicating smaller background errors in the new humidity analysis, also in terms of TCWV. The differences are particularly large in regions that are close to saturation in the background fields (pink contours), by about 2–3 kg/m^2 (the background error itself is 3–6 kg/m^2 in terms of TCWV, not shown). This is consistent with what has been shown earlier in the single-observation experiments.
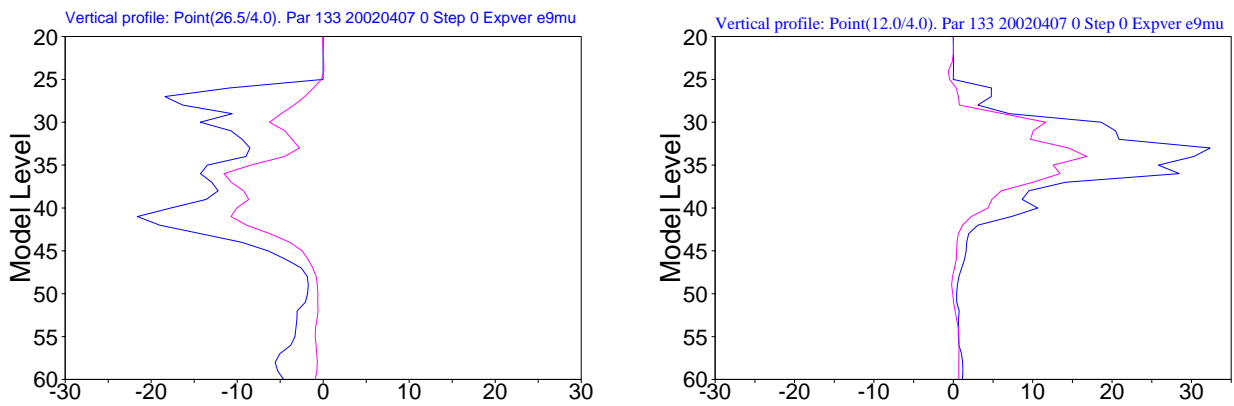
Figure 36: Two selected vertical profiles of humidity increments at a location with negative (left), and positive (right) increment, from a 3D-Var analysis using METEOSAT water-vapour radiance data only, 20020407-00 UTC. The increments are expressed in percent of the background value of q, i.e. $(q^{an} - q^{bg})/q^{bg} * 100$, for the operational (blue) and the re-formulated (magenta) humidity analysis
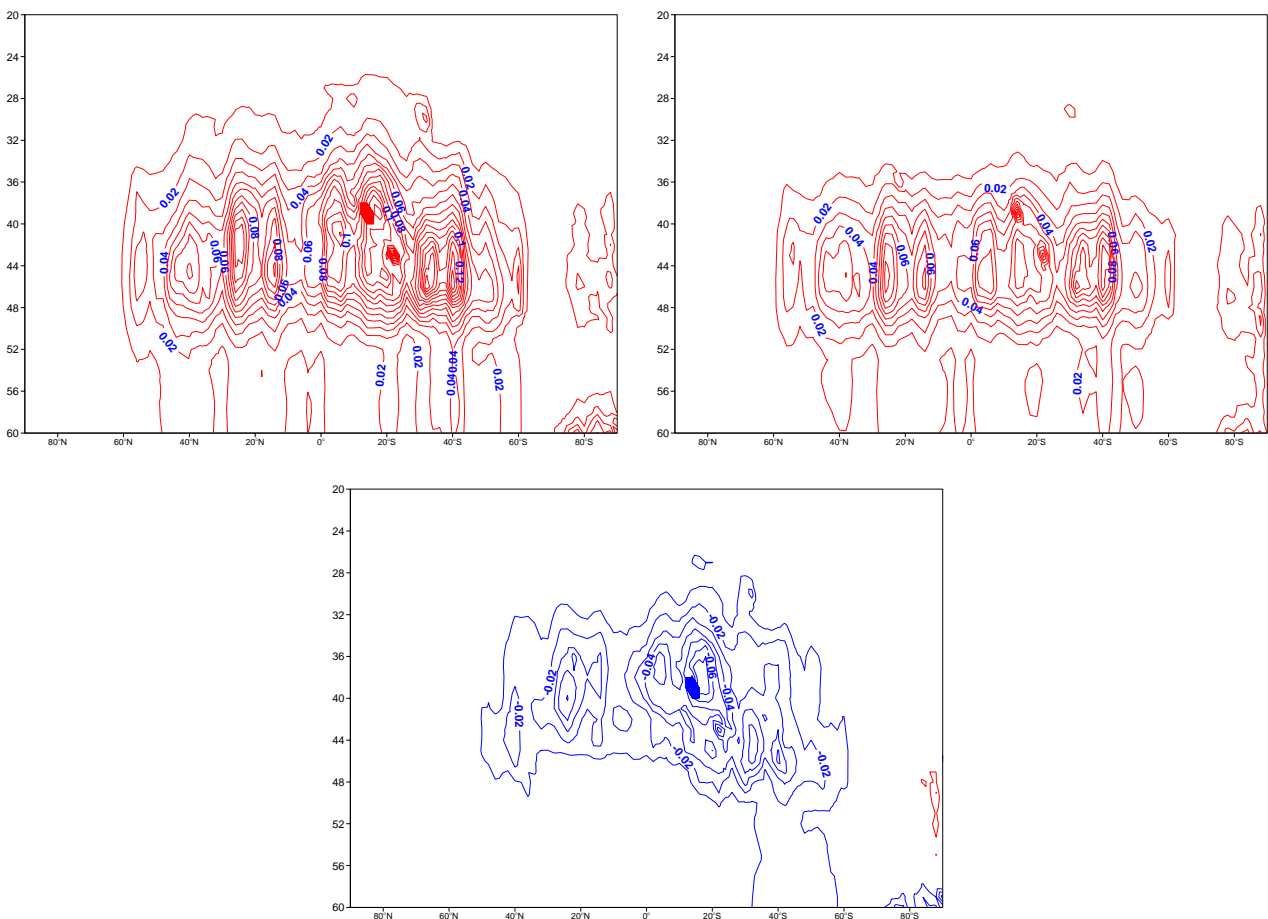

Figure 37: Zonally-averaged analysis humidity increments from a 3D-Var analysis using SSMI radiance data, only, in terms of abs$(q^{an} - q^{bg})/q^{bg}$. The top panels show the current (left) and the revised (right) humidity analysis. The difference between the two (re-formulated minus current) is shown in the lower panel. Contour interval is 0.01.
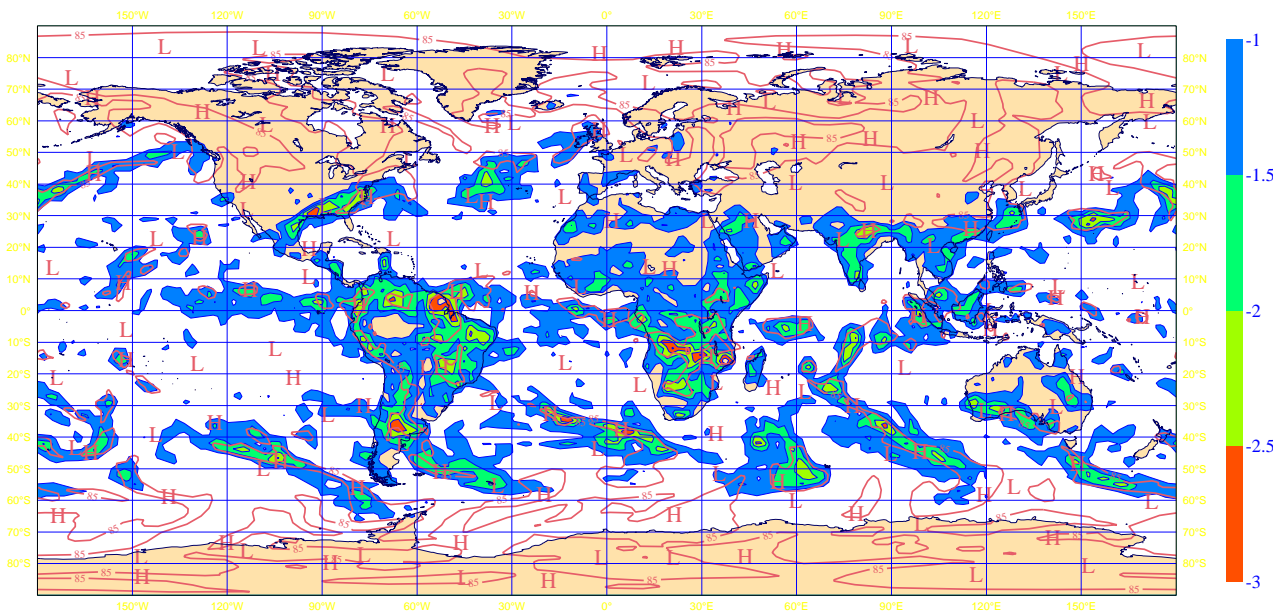
Figure 38: Difference between re-formulated and operational humidity analysis formulation, in terms of TCWV background error standard deviations (kg/m^2), 20020120-00 UTC, computed using the method of Andersson *et al.* (2000). Shading starts at -1.0 kg/m^2 with an interval of 0.5 kg/m^2. The pink contours indicate 85% relative humidity at 700 hPa, in the background fields.

7   Concluding remarks

The current status of assimilation and modelling of the hydrological cycle has been reviewed. The emphasis has been on remote sensing of humidity from current and future satellite systems, in clear-sky, cloudy and precipitating conditions. The improved accuracy and the increasing availability of satellite information on the Earth's hydrological cycle has brought this topic more and more into focus in the last couple of years.

Through comparison with *in-situ* data from several field campaigns, we have shown that the model's performance with respect to boundary-layer humidity is often within the absolute accuracy of most current humidity observing systems (around 5% relative humidity). The biases that exist can therefore be considered relatively small, and the model's performance we consider adequate. From experience with the ERA-40 reanalysis project we have found that these small biases in model and data, nevertheless lead to significant biases in tropical rainfall rate in analyses and short-range forecast. The excess of tropical rainfall shows sensitivity to the assimilation of HIRS infra-red radiances, to the presence of volcanic ash in the atmosphere (e.g. Mt. Pinatubo's eruption in 1994), and to the assimilation of SSMI total-column water-vapour data.

The operational status of satellite remote-sensing of humidity has been presented. Currently, assimilated data include HIRS channel-12, SSMI retrieved TCWV, and METEOSAT water-vapour channel. Later this year the use of SSMI data will be switched to direct 4D-Var assimilation of radiances. The GOES water-vapour channel will be assimilated, as well as additional HIRS channels (partly sensitive to humidity, partly to atmospheric temperature and surface-skin temperature). We reported on the preparations for assimilation of data from AIRS and IASI — the first in a new generation of high spectral-resolution instruments. In particular, this has involved the development of improved fast radiative-transfer models, with a more accurate description of the sensitivity of the radiances with respect to moisture.

A concerted effort is being made to develop the capability for cloud and rain assimilation. Several approaches

have been defined, with the ultimate goal being direct 4D-Var assimilation of cloud- and rain affected radiances. This will involve several new ingredients in the assimilation system, such as linearized moist physical processes, radiative-transfer models including scattering in clouds and precipitation, and enhancements to the 4D-Var system itself — as outlined in Section 5. Single-column retrievals in a 1D-Var framework has shown very encouraging results in a case study of a typhoon.

Several of the above-mentioned aspects of the modelling and assimilation of the hydrological cycle are likely to benefit from the recent development of a re-formulated humidity analysis. The background term of the new formulation takes better account of the wide variability of the humidity background errors. This will improve the interpretation of humidity data, and the inversion of information from radiances to four-dimensional distributions of temperature and humidity. Compared to the background errors in the operational formulation the background errors of the new formulation agree better with statistics of observation-minus-background departures for METEOSAT radiance data.

The chosen humidity control-variable in the new formulation is a normalized relative humidity. At each model gridpoint relative humidity is divided by a polynomial approximation of the background error, which varies as a function of the background relative humidity in the inner loops, with an additional non-linear dependency of the increment itself implemented at the outer loops. This choice of control variable introduces a multivariate relation between the background errors of specific humidity, temperature, and pressure. It is planned to extend the approach further, and incorporate the definition of an uncorrelated humidity control-variable as a way to improve the coupling between the analysed humidity and the dynamic variables (wind temperature and surface pressure).

Ways to reduce inconsistencies between humidity from different observing systems, including an automatic bias correction require further investigation.

8   Acknowledgements

References

Alishouse, J. C., S. A. Snyder, J. Vongsathorn and R. R. Ferraro, 1990: Determination of oceanic total precipitable water from the SSM/I. *IEEE Trans. Geosci. Remote Sensing*, **28,** 811–816.

Andersson, E., J. Pailleux, J.-N. Thépaut, J. Eyre, A. P. McNally, G. Kelly and P. Courtier, 1994: Use of cloud-cleared radiances in three/four-dimensional variational data assimilation. *Q. J. R. Meteorol. Soc.*, **120,** 627–653.

Andersson, E., J. Haseler, P. Undén, P. Courtier, G. Kelly, D. Vasiljevic, C. Branković, C. Cardinali, C. Gaffard, A. Hollingsworth, C. Jakob, P. Janssen, E. Klinker, A. Lanzinger, M. Miller, F. Rabier, A. Simmons,

B. Strauss, J.-N. Théput and P. Viterbo, 1998: The ECMWF implementation of three dimensional variational assimilation (3D-Var). Part III: Experimental results. *Q. J. R. Meteorol. Soc.*, **124,** 1831–1860.

Andersson, E., M. Fisher, R. Munro and A. McNally, 2000: Diagnosis of background errors for radiances and other observable quantities in a variational data assimilation scheme, and the explanation of a case of poor convergence. *Q. J. R. Meteorol. Soc.*, **126,** 1455–1472.

Andersson, E., C. Cardinali, L. Isaksen and A. Garcia-Mendez, 2002: On the impact of frequent data in ECMWF's 4D-Var scheme: Hourly surface pressure data, European profilers and profiling aircraft data. Proc. Eighth Workshop on "Meteorological Operational Systems", ECMWF, Reading, 12–16 November 2001, 179–183.

Bauer, P., 2002: Microwave radiative transfer modelling in cluds and precipitation. Part I: Model description. *NWP-SAF Document No EC-TR-005*.

Bauer, P., J.-F. Mahfouf, W. S. Olson, F. S. Marzano, S. Di Michele, A. Tassa and A. Mugnai, 2002: Error analysis of TMI rainfall estimates over ocean for variational data assimilation. *Q. J. R. Meteorol. Soc.*, **128,** 2129–2144.

Baumgartner, A., and E. Reichel, 1975: The world water balance. *Elsevier*, Amsterdam.

Beljaars, A. C. M., P. Viterbo, M. J. Miller, and A. K. Betts, 1996: The anomalous rainfall over the USA during July 1993: Sensitivity to land surface parametrization and soil moisture anomalies. *Mon. Wea. Rev.*, **124,** 362–383.

Beljaars, A. C. M. and P. Viterbo, 1998: The role of the boundary layer in a numerical weather prediction model. *Clear and cloudy boundary layers*, A. A. M. Holtslag and P. Duynkerke (eds.), Royal Netherlands Academy of Arts and Sciences, Amsterdam, North Holland Publishers, 287–304.

Berre, L., 2000: Estimation of synoptic and mesoscale forecast error covariances in a limited-area model. *Mon. Wea. Rev.*, **128,** 644–667.

Bouttier, F., 2001: The development of 12-hourly 4D-Var. *ECMWF Tech Memo 348*.

Cherubini, T., A. Ghelli, F. Lalaurette, 2001: Verification of precipitation forecasts over the Alpine region using a high density observing network. *ECMWF Tech Memo 340*.

Chevallier, F., P. Bauer, G. Kelly, C. Jakob, and T. McNally, 2001a: Model clouds over oceans as seen from space: comparison with HIRS/2 and MSU radiances *J. Climate*, **14,** 4216–4229.

Chevallier, F., P. Bauer, G. Kelly, J.-F. Mahfouf, C. Jakob, and T. McNally, 2001b: Requirements for the assimilation of cloudy radiances. Proc. ECMWF/EuroTRMM Workshop on "Assimilation of clouds and precipitation", 205–233.

Chevallier, F. and G. Kelly, 2002: Model clouds as seen from space: comparison with geostationary imagery in the 11-μm window region. *Mon. Wea. Rev.*, **130,** 712–722.

Courtier, P., J.-N. Thépaut and A. Hollingsworth, 1994: A strategy for operational implementation of 4D-Var using an incremental approach. *Q. J. R. Meteorol. Soc.*, **120,** 1367–1388.

Courtier, P., E. Andersson, W. Heckley, J. Pailleux, D. Vasiljević, M. Hamrud, A. Hollingsworth, F. Rabier and M. Fisher, 1998: The ECMWF implementation of three dimensional variational assimilation (3D-Var). Part I: Formulation. *Q. J. R. Meteorol. Soc.*, **124,** 1783–1808.

Dee, D. P., and A. M. Da Silva, 2002: On the choice of variable for atmospheric moisture analysis. To appear in *Mon. Wea. Rev.*.

Derber, J. and F. Bouttier, 1999: A reformulation of the background error covariance in the ECMWF global data assimilation system. *Tellus*, **51A,** 195–221.

Douville, H., P. Viterbo, J.-F. Mahfouf A. C. M. Beljaars, 2000: Evaluation of the optimum interpolation and nudging techniques for soil moisture analysis using FIFE data. *Mon. Wea. Rev.*, **128,** 1733–1756.

English, S., and T. J. Hewison, 1998: A fast generic millimetre wave emissivity model. In Proceedings of the SPIE on "Microwave Remote Sensing of the Atmosphere and Environment", **3503**, 22–30.

English, S., D. Jones, A. Smith, F. Hilton and K. Whyte, 2002: ATOVS and SSM/I assimilation at the Met. Office Technical proceedings of the "12th International ATOVS Study Conference", Lorne, Australia, 24 Feb-5 March 2002.

Fillion, L., 2002: Variational assimilation of precipitation data and gravity wave excitation. *Mon. Wea. Rev.*, **130,** 109–124.

Fillion, L. and J.-F. Mahfouf, 2000: Coupling of moist-convective and stratiform precipitation processes for variational data assimilation *Mon. Wea. Rev.*, **128,** 109–124.

Fillion, L. and J.-F. Mahfouf, 2002: Examination of Jacobians of diagnostic and prognostic cloud schemes. Proc. ECMWF/GEWEX Workshop on "Humidity Analysis", Reading, 8–11 July, 2002.

Fisher, M. and E. Andersson, 2001: Developments in 4D-Var and Kalman filtering. *ECMWF Tech Memo 347*.

Garand, L., T. S. Turner, M. Larocque, J. Bates, S. Boukabara, P. Brunel, F. Chevallier, G. Deblonde, R. Engelen, M. Hollingshead, D. Jackson, G. Kedlovec, J. Joiner, T. Kleespies, D. S. McKague, L. McMillin, J-L. Moncet, J. R. Pardo, P. J. Rayer, E. Salathe, R. Saunders, N. A. Scott, P. Van Delst and H. Woolf, 2001: Radiance and Jacobian inter-comparison of radiative transfer modles applied to HIRS and AMSU channels. *J. Geophys. Res.*, **106,** 15pp, In press.

Gérard, E., and R. Saunders, 1999: 4D-Var assimilation of SSM/I total column water vapour in the ECMWF model *Q. J. R. Meteorol. Soc.*, **125,** 3077–3101.

Gregory, D., 1996: Sensitivity of general circulation model performance to convective parametrization. *The physics and parameterization of moist atmospheric convection*, R. K. Smith (ed.), NATO ASI Series C, **505,** Kluwer Academic Press, 463–482.

Harris, B., and G. Kelly, 2001: A satellite radiance bias correction scheme for radiance assimilation. *Q. J. R. Meteorol. Soc.*, **127,** 1453–1468.

Hou, A. Y., S. Q. Zhang, A. M. da Silva, W. S. Olson, C. D. Kummerow, and J. Simpson, 2001: Improving global analysis and short-range forecast using rainfall and moisture observations. *Bull. Amer. Meteor. Soc.*, **82,** 659–679.

Huffman, G. J., R. F. Adler, A. Arkin, A. Chang, R. Ferraro, A. Gruber, J. Janowiak, R. J. Joyce, A. McNab, B. Rudolf, U. Schneider and P. Xie, 1997: The Global Precipitation Climatology Project (GPCP) combined precipitation data set. *Bull. Amer. Meteorol. Soc.*, **78,** 5–20.

Illari, L., 1989: The quality of satellite precipitable water content data and their impact on analyzed moisture fields. *Tellus*, **41A,** 319–337.

Jakob, C. and S. A. Klein, 1999: The role of vertically varying cloud fraction in the parametrization of micro-physical processes in the ECMWF model. *Q. J. R. Meteorol. Soc.*, **125,** 941–965.

Janisková, M., J.-F. Mahfouf, J.-J. Morcrette, and F. Chevallier, 2000: Development of linearized radiation and cloud schemes for the assimilation of cloud properties. *ECMWF Tech Memo 301*.

Janisková, M., 2001: Preparatory studies for the use of observations from the Earth radiation mission in Numerical Weather Prediction. *ESA Contract Report*, 13151/98/NL/GD.

Janisková, M., J.-F. Mahfouf and J.-J. Morcrette, 2002: Preliminary studies on the variational assimilation of cloud-radiation observation. To appear in *Q. J. R. Meteorol. Soc.*.

Köpken, C., 2001: Monitoring of METEOSAT WV radiances and solar stray light effects. *EUMET-SAT/ECMWF Fellowship Programme Research Report*, **10,** pp 46.

Köpken, C., G. Kelly and J.-N. Thépaut, 2002: Monitoring and assimilation of METEOSAT radiances within the 4D-Var system at ECMWF. *EUMETSAT/ECMWF Fellowship Programme Research Report*, **9,** pp 31.

Kummerow, C., W. Barnes, T. Kozu, J. Shiue and J. Simpson, 1998: The Tropical Rainfall Measuring Mission (TRMM) sensor package. *J. Atmos. Oceanic. Technol.*, **15,** 809–817.

Lorenc, A. C., S. P. Ballard, R. S. Bell, N. B. Ingleby, P. L. F. Andrews, D. M. Barker, J. R. Bray, A. M. Clayton, T. Dalby, D. Li, T. J. Paine, and F. W. Saunders, 2000: The Met. Office global three-dimensional variational data assimilation scheme. *Q. J. R. Meteorol. Soc.*, **126,** 2991–3012

Macpherson, B., 2001: Operational experience with assimilation of rainfall data in the Met. Office mesoscale model. *Meteorol. Atmos. Phys.*, **76,** 3–8.

Marécal, V. and J.-F. Mahfouf, 2000: Variational retrieval of temperature and humidity profiles from TRMM precipitation data *Mon. Wea. Rev.*, **128,** 3853–3866.

Marécal, V. and J.-F. Mahfouf, 2002a: Four-dimensional variational assimilation of total column water vapour in rainy areas. *Mon. Wea. Rev.*, **130,** 43–58.

Marécal, V. and J.-F. Mahfouf, 2002b: Experiments on 4D-Var assimilation of rainfall data using an incremental formulation. *ECMWF Tech Memo 367*.

Marécal, V., J.-F. Mahfouf, and P. Bauer, 2002: Comparison of TMI rainfall estimates and their impact on 4D-Var assimilation. *ECMWF Tech Memo 364*, 20pp.

Marécal, V., É. Gérard, J.-F. Mahfouf, and P. Bauer, 2000: The comparitive impact of the assimilation of SSM/I and TMI brightness temperatures in the ECMWF 4D-Var system. *ECMWF Tech Memo 302*.

Matricardi, M. and R. Saunders, 2001: A fast radiative transfer model for simulation of IASI radiances. *ECMWF Tech Memo 324*.

Matricardi, M., F. Chevallier and S. Tjemkes, 2001: An improved general fast radiative transfer model for the assimilation of the radiance observations. *ECMWF Tech Memo 345*.

McNally, A. P., and M. Vesperini, 1996: Variational analysis of humidity information from TOVS radiances *Q. J. R. Meteorol. Soc.*, **122,** 1521–1544.

McNally, A. P., E. Andersson, G. A. Kelly and R. W. Saunders, 1999: The use of raw TOVS/ATOVS radiances in the ECMWF 4D-Var assimilation system. *ECMWF Newsletter*, **83,** 2–7.

Moreau, E., P. Bauer and F. Chevallier, 2002: Microwave radiative transfer modelling in cluds and precipitation. Part II: Model evaluation. *NWP-SAF Document No EC-TR-006.*

New, M, M. Hulme and P. Jones, 2000: Representing twentieth-century space-time climate variability. Part II: Development of 1901–96 monthly grids of terrestrial surface climate. *J. Climate*, **13,** 2217–2238.

Phallipou, L., 1993: A microwave radiative transfer model. *ECMWF Tech Memo 190.*

Phallipou, L., 1996: Variational retrieval of humidity profile, wind speed and cloud liquid water path with the SSM/I: Potential for numerical weather prediction. *Q. J. R. Meteorol. Soc.*, **122,** 327–355.

Purser, R. J., W.-S. Wu, D. F. Parrish and N. M. Roberts, 2002: Numerical aspects of the application of recursive filters to variational analysis. Part II: spatially inhomogeneous and anisotropic general covariances. Submitted to *Mon. Wea. Rev..*

Rabier, F., A. McNally, E. Andersson, P. Courtier, P. Undén, J. Eyre, A. Hollingsworth and F. Bouttier, 1998: The ECMWF implementation of three dimensional variational assimilation (3D-Var). Part II: Structure functions. *Q. J. R. Meteorol. Soc.*, **124,** 1809–1829.

Rabier, F., H. Järvinen, E. Klinker, J.-F. Mahfouf and A. Simmons, 2000: The ECMWF operational implementation of four dimensional variational assimilation. Part I: Experimental results with simplified physics. *Q. J. R. Meteorol. Soc.*, **126,** 1143–1170.

Rodgers, C. D., 2000: *Inverse methods for atmospheric sounding: Theory and practice.* Series on atmospheric, Oceanic and Planetary Physics, **2,**.

Rudolf, B., H. Hauschild, W. Rüth, and U. Schneider, 1996: Comparison of rain gauge analyses, satellite-based precipitation estimates and forecast model results. *Adv. Space. Res.*, **7,** 53–62.

Saunders, R., M. Matricardi and P. Brunel, 1999: An improved fast radiative transfer model for assimilation of satellite radiance observations. *Q. J. R. Meteorol. Soc.*, **125,** 1407–1426.

Siebesma, P. and C. Jakob, 2002: Decision making in a bulk mass-flux convection parametrization. Influence on triggering, updraught properties and model climate. In press.

Simmons, A., A. Untch, C. Jakob, P. Kållberg and P. Undén, 1999: Stratospheric water vapour and tropical tropopause temperatures in ECMWF analyses and multi-year simulations. *Q. J. R. Meteorol. Soc.*, **125,** 353–386.

Simpson, J., C. Kummerow, W.-K. Tao and R. F. Adler, 1996: On the Tropical Rainfall Measuring Mission (TRMM). *Meteorol. Atmos. Phys.*, **60,** 19–36.

Simmons, A. J. and A. Hollingsworth, 2002: Some aspects of the improvement in skill of numerical waether prediction. *Q. J. R. Meteorol. Soc.*, **128,** 647–678.

Tiedtke, M., W. A. Heckley, and J. Slingo, 1988: Tropical forecasting at ECMWF: The influence of physical parametrization on the mean structure of forecasts and analyses. *Q. J. R. Meteorol. Soc.*, **114,** 639–665.

Tiedtke, M., 1989: A comprehensive mass flux scheme for cumulus parameterization in large-scale models. *Mon. Wea. Rev.*, **117,** 1779–1800.

Tiedtke, M., 1993: Representation of Clouds in Large-Scale Models. *Mon. Wea. Rev.*, **121,** 3040–3061.

Treadon, R. E., 1997: Assimilation of satellite derived precipitation estimates with the NCEP GDAS. *PhD dissertation*, The Florida State University, pp 348.

Tsuyuki, T., 1997: Variational data assimilation in the Tropics using precipitation data. Part III: Assimilation of SSM/I precipitation rates. *Mon. Wea. Rev.*, **125,** 1447–1464.

Van den Hurk, B. J. J. M., P. Viterbo, A. C. M. Beljaars and A. K. Betts, 2000: Offline validation of the ERA40 surface scheme. *ECMWF Tech Memo 295*.

Viterbo, P. and A. C. M. Beljaars, 1995: An improved land surface parametrization scheme in the ECMWF model and its validation. *J. Climate*, **8,** 2716–2748.

Viterbo, P. and P. Courtier, 1995: The importance of soil water for medium-range weather forecasting, implications for data assimilation. WMO workshop on Imbalances of slowly varying components of predictable atmospheric motions, Beijing, China, 121–130.

Weaver, A. T. and P. Courtier, 2001: Correlation modelling on the sphere using a generalized diffusion equation. *Q. J. R. Meteorol. Soc.*, **127,** 1815–1846.

Weller, R. A. and S. P. Anderson, 1996: Surface meteorology and air-sea fluxes in the western equatorial Pacific warm pool during the TOGA Coupled Ocean-Atmosphere Response Experiment (COARE). *J. Climate*, **9,** 1959–1990.

Xie, P., and P. Arkin, 1997: Global precipitation: A 17-year monthly analysis based on gauge observations, satellite estimates and numerical model outputs. *Bull. Amer. Meteorol. Soc.*, **78,** 2539–2558.